Electronic structure of transition-atom impurities in GaP

V. A. Singh* and Alex Zunger

Solar Energy Research Institute, Golden, Colorado 80401
and Department of Physics, University of Colorado, Boulder, Colorado 80309
(Received 14 June 1984)

We describe the elements of the electronic structure and the chemical trends in cation-substitutional Cr, Mn, Fe, Co, Ni, Cu, and Zn impurities in GaP and Fe in InP. First, using the recently developed method of Fazzio, Caldas, and Zunger, we deconvolute the observed acceptor, donor, and intracenter $d \rightarrow d^*$ excitation energies into a one-electron mean-field contribution and a many-electron multiplet correction. Then, using the self-consistent quasiband crystal-field Green's-function method of Lindefelt and Zunger, we show that one-electron theory explains the magnitudes and the trends in the mean-field part of the observed transition energies (evaluated as differences in total energies). Many-electron contributions are found to be sizable, and are responsible for the non-monotonic trends of the observed acceptor energies with the impurity's atomic number and a reduction in the Mott-Hubbard Coulomb energies. We discuss in detail the impurity-induced energy levels (gap states as well as resonances), the photoionization and intracenter excitations, the attenuation of the Mott-Hubbard Coulomb repulsion energies with the attendant plurality of charge states, the self-regulating response of the electron density to excitations, and the nature of the transition-atom—host chemical bond with its relationship to the structure of bulk $3d$ phosphides.

I. INTRODUCTION

The utility of III-V—compound semiconductors in many device applications, ranging from high-speed logic circuits,[1,2] optoelectric devices,[3,4] microwave devices,[5] and solar cells,[6] rests on the characteristics of the intentionally introduced impurities (dopants) as much as it depends on the properties of trace amounts of unintentional contaminations. Transition-atom (TA) impurities in compound semiconductors form a special class of such contaminants. They were studied experimentally in great detail (e.g., review articles in Refs. 7 and 8) using a broad range of techniques, including optical absorption, luminescence, photocapacitance, photoconductivity, electron paramagnetic resonance (EPR), electron-nuclear double resonance (ENDOR), deep-level transient spectroscopy (DLTS), and Hall effect. This article is concerned with the theoretical understanding of the electronic properties of perhaps the experimentally most studied system in this group: TA impurities in GaP. The Appendix[9−52] and Figs. 1(a), 2(a), 3(a), 4(a), and 5(a) summarize the most reliably determined levels of GaP:TA, for TA = Cr, Mn, Fe, Co, and Ni (GaP:Zn gives rise to only a simple shallow acceptor, and GaP:Cu shows mostly complexes). Detailed EPR and ENDOR studies[7,8] suggest that with one possible exception (neutral[34] and doubly negative[36] Fe in GaP, for which no conclusive data exist as yet), all $3d$ elements considered take up a cation substitutional site in GaP, much like the situation in other III-V compounds[7,8,53] (e.g., InP and GaAs) and the II-VI compounds[52] (e.g., ZnS and ZnSe), but in contrast with the situation in Si, where under normal diffusion conditions the tetrahedral interstitial site is often favored.[53(a)]

Few of the elements of the structural and electronic properties of GaP:TA can be appreciated from a cursory look at the experimental data and from simple atomic considerations. When a transition atom takes up the trivalent Ga site, its formal oxidation state becomes that of Ga, i.e., T^{3+} for a neutral center, T^{2+} for a singly negatively charged center, and T^{4+} for a positively charged center. Assume first that the crystalline environment was a weak perturbation on these oxidation states of the transition-atom impurity and examine the consequences of this assumption *vis-à-vis* experiments. Figure 6 displays the calculated[54] $3d$-orbital energies of the free ions Ni through V in these three oxidation states. We give both the spin-up (d_+) and the spin-down (d_-) energies; their separation (shaded area in Fig. 6) is the exchange splitting. First, observe that the orbital energies become less negative with decreasing impurity atomic number Z, going from Ni to V (a Coulomb attraction effect). The slope of this reduction in binding energies is about 1—3 eV per unit increment in Z. Since this is also the order of magnitude of the semiconductor band gap (shown schematically at the top of Fig. 6), at this rate there will be at most one impurity that would have its level inside the semiconductor band gap. In fact, all impurities shown in Fig. 6 were observed experimentally to have band-gap levels in GaP [Appendix and Figs. 1(a)—5(a)] as well as in InP and GaAs.[7,8] Second, note that the binding energy increases rapidly as the oxidation state changes from 2 + to 3 + and 4 +, at a rate of about 15—20 eV per unit increment in the oxidation number. This is related to the (Mott-Hubbard) single-site Coulomb repulsion effect; interelectronic repulsions of the order $U \approx 15$—20 eV are characteristic of $3d$ atoms.[55] At this rate, if a level of a particular transition atom does exist inside the semiconducting gap, it will have at most a single stable oxidation state (say, T^{4+} in a nomenclature scheme to be explained in the following section), and will be pushed into
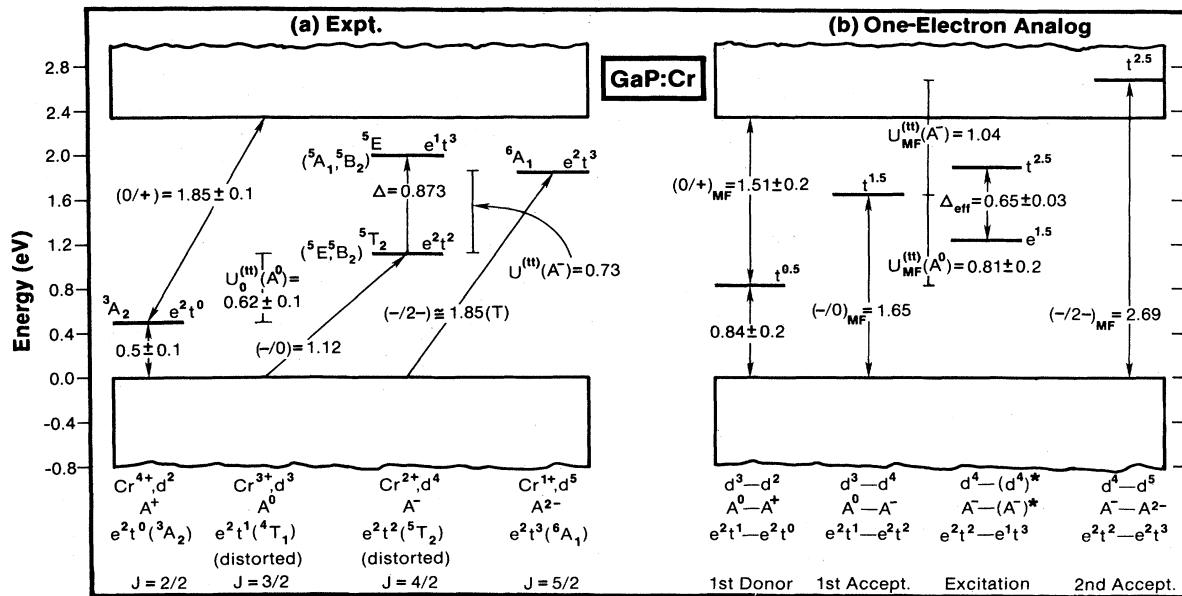
FIG. 1. (a) Experimentally observed donor, acceptor, and intra-d excitations in GaP:Cr, and the theoretical assignments of the multiplet states and dominant one-electron configurations. See Appendix, subsection 1, for details and references. T denotes tentative values. (b) One-electron mean-field analog for donor, acceptor, and intra-d excitations in GaP:Cr.

the conduction band when a second electron is captured (producing T^{3+}). Similarly, if a level will exist in GaP (i.e., T^{3+} when neutral) it would not exist in ZnS (T^{2+} when neutral). In fact, the experimental data summarized in Figs. 1(a)—5(a) show that, for GaP, the impurities Mn and Co exist in the gap in two oxidation states, Fe and Ni exist in three oxidation states, and Cr has been observed to

exist in four oxidation states. Furthermore, these impurities give rise to band-gap levels both when replacing trivalent host cations (e.g., GaP) or divalent host cations[7,8] (e.g., ZnS). Indeed, for this to occur, the Coulomb repulsion energies of the free ions would have to be reduced in the solid by 1—2 orders of magnitude, i.e., $U \sim 0.2$—2 eV. This is surprising since EPR and ENDOR measurements
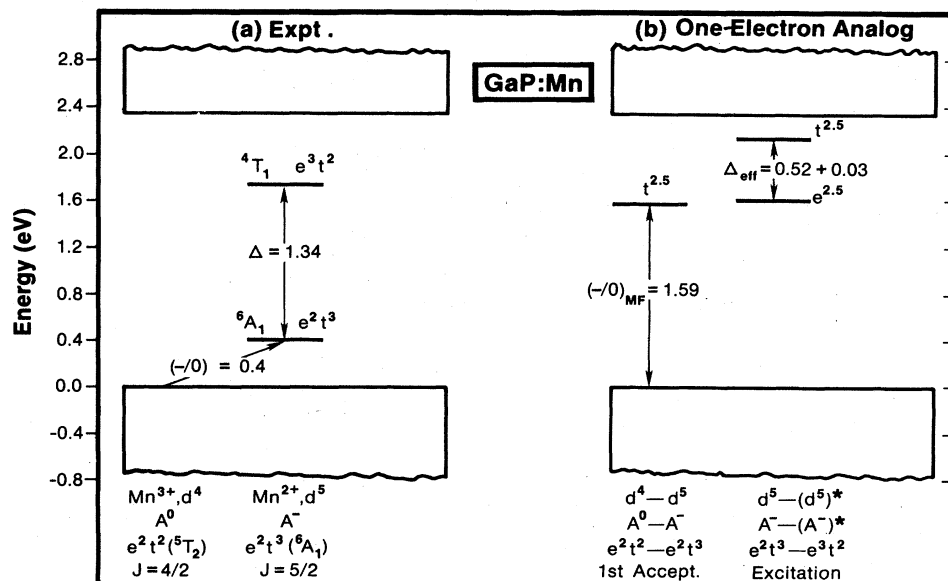

FIG. 2. Same as Fig. 1, for GaP:Mn; see Appendix, subsection 2, for details and references.
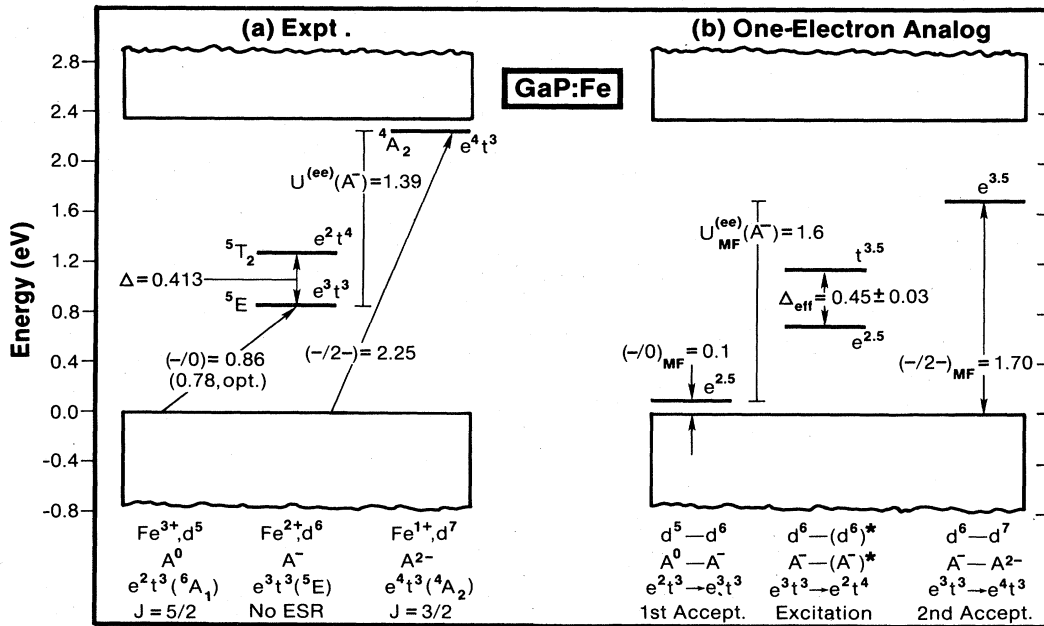
FIG. 3. Same as Fig. 1, for GaP:Fe; see Appendix, subsection 3, for details and references.

suggest that these impurities have localized orbitals resembling atomic $3d$ orbitals. Hence, much like the situation in biological electron-transporting molecules,[56] (e.g., Cytochrome C), where the different oxidation states of the transition atom (i.e., Fe) are separated by less than 1 eV, so are the different ionization states of a TA compressed into a narrow band-gap range when they exist as impurities in semiconductors. Third, the absorption spectra of GaP:TA at sub-band-gap photon energies show sharp

lines,[7,8] resembling the familiar multiplet transitions in free atoms,[57] except that the energy range of the spectra is compressed by about a factor of 10. Fourth, whereas the free-ion orbital ionization energies of Fig. 6 show a change in slope of 2.5 eV between high-spin ionizations and low-spin ionizations (Mn^{2+} d^5 and Fe^{2+} d^6, respectively), the change is 5 times smaller for the corresponding impurities (0.45 eV between the Mn and Fe first acceptors, cf. Figs. 2 and 3). Finally, EPR (Refs. 7 and 8)
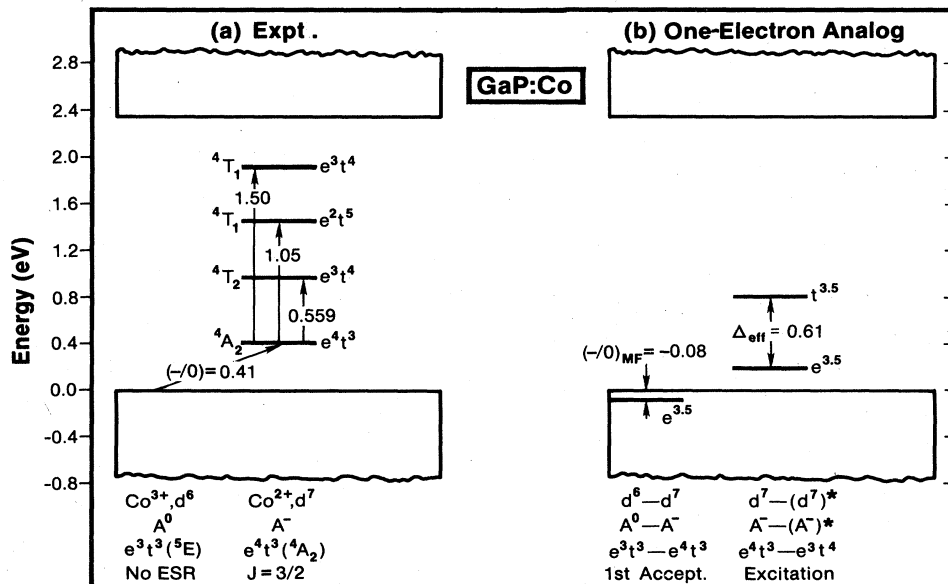

FIG. 4. Same as Fig. 1, for GaP:Co; see Appendix, subsection 4, for details and references.
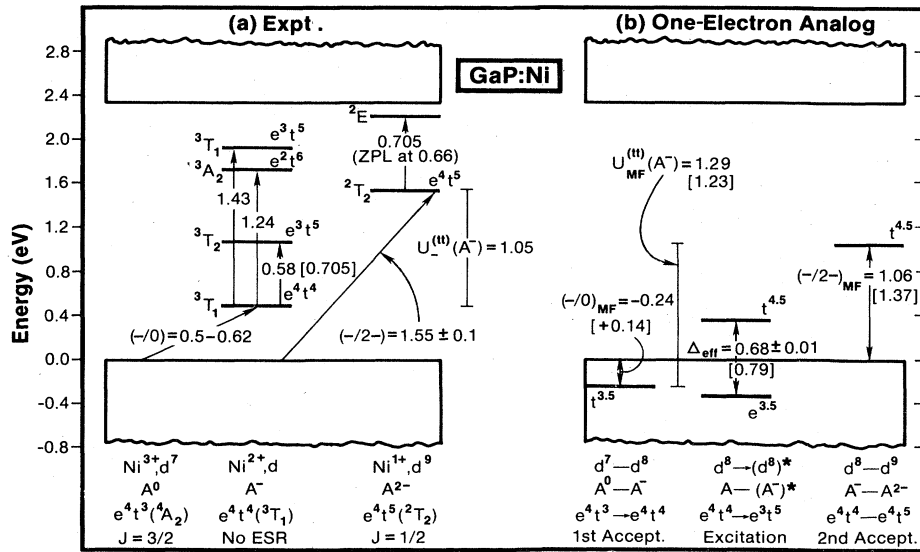
FIG. 5. Same as Fig. 1, for GaP:Ni. Here we give two sets of experimental data for the $^3T_1 \rightarrow ^3T_2$ intracenter excitations (discussed in Appendix, subsection 5), and the corresponding two sets of the calculated mean-field values.

shows these systems to occur at their maximum spin [J in Figs. 1(a)—5(a)], and hence, despite the fact that interelectronic repulsions are reduced substantially in the solid, the exchange splittings (2—5 eV in ions, cf. Fig. 6) must necessarily remain reasonably high to prefer the (Hund's-rule) high-spin ground state. One concludes that

FIG. 6. Calculated (local spin density, cf. Ref. 54) orbital energies for free ions of transition- (T) metal elements. At the top we give, for comparison of scale, the energy gaps of three semiconductors. The shaded areas (exchange splitting) separate the spin-up (d_+) from the spin-down (d_-) orbital energies. Ionizations take place form the highest occupied orbital, e.g., for T^{2+} it involves the lower d_+ orbital for V, Cr, and Mn, and then the upper d_- orbital for Fe, Co, and Ni. Hence, orbital ionizations show a slope discontinuity with a (local) minimum at Mn and (local) maximum at Fe.

the GaP:TA system appears to show a dual behavior with respect to localization: It is sufficiently localized to maintain a large enough exchange splitting and a multiplet structure, but it is sufficiently delocalized to exhibit small Coulomb repulsions with the attendant plurality of charge states, a compressed excitation spectrum, and a slow reduction in binding energies with decreasing Z.

From these simple observations one concludes that a theory is needed for explaining the *chemical shift* in binding energies (i.e., reduction of their slope with Z), the *Coulomb reduction* (i.e., the attenuation of repulsion energies by 1—2 orders of magnitude), and the survival of the *many-electron multiplet effects* in the solid, with their attendant high-spin ground states. In this first self-consistent study of transition-atom impurities in an extended compound semiconductor we set out to clarify these issues.

The strategy that we adopt in this work is as follows. First, using the recently developed method of Fazzio, Caldas, and Zunger,[52] we will resolve the experimental excitation and ionization energies ΔE into a mean-field (MF) one-electron part ΔE_{MF} and a multiplet correction (MC) part ΔE_{MC}. This is needed since the local-density approach underlying our work cannot handle conveniently the multiplet part, except for its spin contribution (when carried in a spin-polarized fashion). Not knowing in advance if spin correlations are more important than space correlations, we circumvent this problem by determining ΔE_{MC} directly from experiment through a theoretical model.[52] We next use self-consistent one-electron theory to independently calculate the MF contribution $\Delta E_{MF} = \Delta E - \Delta E_{MC}$ from the electronic structure. We represent this energy as the difference between the total MF energies of the final and initial configurations. Since local-density eigenvalues do not correspond to removal energies,[54] we evaluate ΔE_{MF} from differences in total energies (through the transition-state construct, see below). This is achieved by solving self-consistently for the elec-
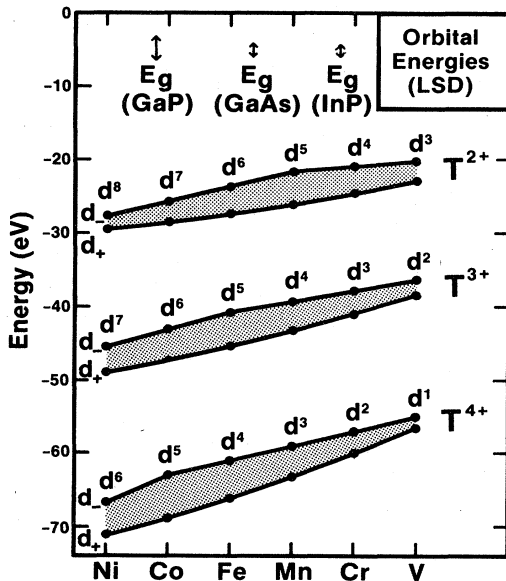
tronic structure of an impurity in an infinite host crystal, using a series of electronic configurations, one at the time, appropriate for the various transitions. We use for this purpose the first-principles quasiband crystal-field (QBCF) Green's-function method of Lindefelt and Zunger.[58] It provides highly accurate self-consistent solutions to the problem within the local-density framework. We have previously shown the highly stable convergence properties of this method,[58,59] have demonstrated that when applied to problems treated by other first-principles Green's-function methods[60(a),60(b)] (the Si vacancy (Ref. 58) and Si:S (Ref. 61), and Si:Zn [(Ref. 59(a)]) the same results are reproduced. We have further applied it to numerous other systems (O, S, and Se in Si,[61] substitutional[59] and interstitial[62(a)−62(c)] $3d$ impurities in silicon, comparison of Cu, Ag, and Au impurities in silicon[59(e)]), for which no application with any first-principles Green's-function method exist. Finally, we show that the calculated ΔE_{MF} excitation and ionization energies reproduce those deduced from experiment, and discuss discrepancies, where they exist, in terms of lattice-distortion effects. Based on the accuracy of our results, we analyze in detail quantities not delivered directly through experimental probing, such as impurity-induced resonances, the charge distribution in the system, and its implication in the nature of the impurity-host chemical bond. This provides the first comprehensive picture of the physical and chemical elements underlying transition-atom impurities in GaP.

II. NOMENCLATURE

The chemical nomenclature used in this field to designate various charge and oxidation states is often confusing. We briefly define here this notation and discuss its implications.

If an isolated neutral (A^0) transition atom has a one-electron configuration $d^p s^q$, then when it takes up a trivalent substitutional site (e.g., the Ga site in GaP) its oxidation state is denoted T^{3+} and its formal configuration is denoted $d^N = d^{p+q-3}$. If singly positive (A^+), its oxidation state is T^{4+} and its formal configuration is $d^N = d^{p+q-4}$. If singly negative (A^-), its oxidation state is T^{2+} and its formal configuration is $d^N = d^{p+q-2}$. This

nomenclature is summarized in Table I. While this notation is borrowed historically from the field of ionic coordination compounds,[63,64] where the oxidation state symbolizes a complete ionic charge transfer (i.e., T^{3+} is imagined as having one less electron than T^{2+} on the impurity site), we will use it here merely as a convenient formal notation, without implying by it the nature of the impurity-host bonding. The latter issue will be addressed in some detail in our electronic structure calculations (Sec. VI D), where a different picture emerges.

The experimental findings summarized in the Appendix show that all $3d$ impurities exist in GaP as neutral centers [denoted (A^0, T^{3+}, d^{p+q-3})], whereas Cr, Fe, and Ni exist also as doubly negatively charged centers [denoted (A^{2-}, T^{1+}, d^{p+q-1})], and Cr exists also as a positively charged center [denoted (A^+, T^{4+}, d^{p+q-4})].

Elementary considerations of crystal-field theory[53] also indicate that the symbolic configuration "d^N" actually exists in the cubic impurity system as two impurity-induced levels: an e level (fourfold degenerate, including spin) and a t_2 level (sixfold degenerate, including spin), where the one-electron configuration is $e^m t^n$ with $n + m = N$. Electronic transitions in these systems involve configuration changes, often denoted as $e^m t^n \rightarrow e^{m'} t^{n'}$. We next discuss the two types of electronic transitions observed in such systems.

III. TWO TYPES OF ELECTRONIC TRANSITIONS IN GaP:TA

Absorption, luminescence, Hall-effect, and photoconductivity experiments indicate two types of electronic transitions in this system: those that occur within a fixed formal charge state and those that alter the formal charge state of the center.

A. Intracenter $d \rightarrow d^*$ excitations

The intracenter transitions are excitations within a fixed formal charge where the configuration of the impurity $e^m t^n$ changes to $e^{m-1} t^{n+1}$ or $e^{m+1} t^{n-1}$, etc. They are often referred to as $d^N \rightarrow (d^N)^*$ internal transitions, or crystal-field excitons, and resemble similar transitions in the free ions,[57] where both initial and final state belong to

TABLE I. Nomenclature used to describe the charge state (A^0, A^-, and A^{2-}), the oxidation states (T^{3+}, T^{2+}, and T^{1+}, respectively), and the symbolic configuration (d^n, d^{n+1}, d^{n+2}, respectively) of substitutional $3d$ impurities on a trivalent cation site in III—V compound semiconductors.

Impurity	Free-atom configuration	Neutral impurity (A^0)		Negative impurity (A^-)		Doubly negative impurity (A^{2-})	
		Symbolic configuration	Oxidation state	Symbolic configuration	Oxidation state	Symbolic configuration	Oxidation state
V	$d^3 s^2$	d^2	V^{3+}	d^3	V^{2+}	d^4	V^{1+}
Cr	$d^5 s^1$	d^3	Cr^{3+}	d^4	Cr^{2+}	d^5	Cr^{1+}
Mn	$d^5 s^2$	d^4	Mn^{3+}	d^5	Mn^{2+}	d^6	Mn^{1+}
Fe	$d^6 s^2$	d^5	Fe^{3+}	d^6	Fe^{2+}	d^7	Fe^{1+}
Co	$d^7 s^2$	d^6	Co^{3+}	d^7	Co^{2+}	d^8	Co^{1+}
Ni	$d^8 s^2$	d^7	Ni^{3+}	d^8	Ni^{2+}	d^9	Ni^{1+}
Cu	$d^{10} s^1$	d^8	Cu^{3+}	d^9	Cu^{2+}	d^{10}	Cu^{1+}
Zn	$d^{10} s^2$	d^9	Zn^{3+}	d^{10}	Zn^{2+}		
Ga	$d^{10} s^2 p^1$	d^{10}	Ga^{3+}				

the same formal charge (and hence oxidation) state. The change in the total many-electron energy E_T attendant upon such transitions is denoted as

$$\Delta^{(ij)} = E_T^{(j)}[e^{m'}t^{n'}] - E_T^{(i)}[e^m t^n] , \qquad (1)$$

where $E_T^{(j)}[e^{m'}t^{n'}]$ and $E_T^{(i)}[e^m t^n]$ are, respectively, the total energies of multiplets $|j\rangle$ and $|i\rangle$ (only the multiplet representation indices i and j are the appropriate quantum numbers for these many-electron states. We include in this paper the predominant one-electron configurations $e^{m'}t^{n'}$ and $e^m t^n$ only as a reminder that different multiplets correspond to different configurations).

Since both the excited electron and the hole left behind remain, in most cases, partially bound, the excitation energy of Eq. (1) contains an electron-hole excitonic contribution, much like in the case of $3d$ core excitons in semiconductors.[59(d)] The experimental findings surveyed in the Appendix show that in GaP:$M^{(3d)}$ such intracenter excitations can be observed only for the (A^-, T^{2+}, d^{p+q-2}) center, the only exception being Ni, which shows also an intracenter transition of the $(A^{2-}, \text{Ni}^{1+}, d^9)$ center. The excited states of A^0 may be overlapping with the photoionization transitions and are usually not resolved. The number of intracenter transitions is limited by the size of the band gap E_g; hence only a rather small number of transitions are observed in GaP ($E_g = 2.35$ eV), compared with wider-gap materials such as ZnS or NiO (none were observed so far in silicon). Specifically, in GaP a single intracenter transition has been observed for the Cr, Mn, and Fe impurities, and three transitions have been observed for Co and Ni impurities. A glance at Figs. 1(a)–5(a) shows that the excitation energies for these intracenter transitions are almost an order of magnitude smaller than the corresponding transitions in the free ions.[57] On the other hand, they are about an order of magnitude larger than the $Ns \rightarrow np$ intracenter excitations of effective-mass-like impurities.

B. Ionizations

Whereas intracenter excitations are charge conserving, the second type of electronic transitions characterizing GaP:TA ("charge-transfer") thermal ionizations or photoionizations) changes the formal charge state of the center. We refer to these as ionizations, although the removed electron or added hole remains in the crystal and can have a finite amplitude on the excited atom.[59(d)] Few types of such ionization processes are pertinent here.

1. Single (first) acceptors

The single-acceptor ionizations correspond to the process where, for example, a valence-band (VB) electron is transferred to an impurity level of type e or t, changing thereby the charge state from A^0 to A^-. If the fully occupied valence band has M electrons, such single-acceptor ionization (a reduction reaction) can be described as

$$A^0, (\text{VB})^M t^n \rightarrow A^-, (\text{VB})^{M-1} t^{n+1}$$

or $\qquad (2)$

$$A^0, (\text{VB})^M e^m \rightarrow A^-, (\text{VB})^{M-1} e^{m+1} .$$

This type of single-acceptor process is often referred to as hole emission to the valence band, and the associated change in the total free energy E_T of the system is denoted as $H(-/0)$, i.e.,

$$H^{(t)}(-/0) = E_T^{(j)}[A^-, (\text{VB})^{M-1} t^{n+1}] - E_T^{(i)}[A^0, (\text{VB})^M t^n] ,$$

or $\qquad (3)$

$$H^{(e)}(-/0) = E_T^{(j')}[A^-, (\text{VB})^{M-1} e^{m+1}]$$
$$- E_T^{(i')}[A^0, (\text{VB})^M e^m] ,$$

where each total-energy term corresponds to the lowest multiplet $(i, j, i', \text{ or } j')$ of the corresponding charge state.

A complementary acceptor ionization process can occur where a conduction-band (CB) electron is captured by an impurity center. This can be described as an electron-capture process:

$$A^0, (\text{CB})^1 t^n \rightarrow A^-, (\text{CB})^0 t^{n+1}$$

or $\qquad (4)$

$$A^0, (\text{CB})^1 e^m \rightarrow A^-, (\text{CB})^0 e^{m+1} .$$

2. Double (second) acceptors

Double-acceptor ionizations correspond to a process where a second valence-band electron is transferred to the impurity levels, changing thereby the charge state from A^- to A^{2-}. This can be described as a second hole emission process:

$$A^-, (\text{VB})^M t^{n+1} \rightarrow A^{2-}, (\text{VB})^{M-1} t^{n+2}$$

or $\qquad (5)$

$$A^-, (\text{VB})^M e^{m+1} \rightarrow A^{2-}, (\text{VB})^{M-1} e^{m+2} .$$

The change in total free energy attendant upon this process can be denoted as $E(-/2-)$, or

$$E^{(t)}(-/2-) = E_T^{(j)}[A^{2-}, (\text{VB})^{M-1} t^{n+2}]$$
$$- E_T^{(i)}[A^-, (\text{VB})^M t^{n+1}]$$

and $\qquad (6)$

$$E^{(e)}(-/2-) = E_T^{(j')}[A^{2-}, (\text{VB})^{M-1} e^{m+2}]$$
$$- E_T^{(i')}[A^-, (\text{VB})^M e^{m+1}] .$$

Again, the complementary process of capture of a second electron from the conduction band is possible (but less likely).

3. Single (first) donors

Single-donor ionization (an oxidation reaction) corresponds to a process where the impurity level emits an electron to the conduction band, changing the formal charge state from A^0 to A^+. This can be described as

$$A^0, (\text{CB})^0 t^n \rightarrow A^+, (\text{CB})^1 t^{n-1}$$

or $\qquad (7)$

$$A^0, (\text{CB})^0 e^m \rightarrow A^+, (\text{CB})^1 e^{m-1} .$$

The change in total free energy attendant upon this electron emission is denoted as $E(0/+)$ and given by

$$E^{(t)}(0/+)=E_T^{(j)}[A^+,(\text{CB})^1 t^{n-1}]-E_T^{(i)}[A^0,(\text{CB})^0 t^n]$$

or (8)

$$E^{(e)}(0/+)=E_T^{(j')}[A^+,(\text{CB})^1 e^{m-1}]-E_T^{(i')}[A^0,(\text{CB})^0 e^m] .$$

The complementary process of a single-donor transition through a hole capture by the valence band is possible (although less likely) and can be described as

$$A^0,(\text{VB})^{M-1}t^n \to A^+,(\text{VB})^M t^{n-1}$$

or (9)

$$A^0,(\text{VB})^{M-1}e^m \to A^+,(\text{VB})^M e^{m-1} .$$

Double-donor transitions can be constructed in analogy with the single-donor electron-emission process.

C. Mott-Hubbard Coulomb energies

Using the above definition of donor and acceptor energies, one can further define the apparent Mott-Hubbard Coulomb repulsion energy $U^{(\alpha\beta)}$ as the energy required to transfer an impurity electron from orbital α on one site and place it in orbital β on a distant impurity site. Clearly, this definition implies that U includes (i) frozen-lattice one-electron effects including changes in screening, polarization, and crystal-field splittings attendant upon charge exchange, (ii) many-electron multiplet effects, and (iii) lattice-relaxation effects. The contribution of (i) is positive, whereas (ii) and (iii) can be either positive or negative. If we carry out this process for the neutral center A^0, we first remove an electron from orbital α to form A^+, investing an energy $E^{(\alpha)}(0/+)$ [Eq. (8)], and then we add an electron to orbital β on a distant neutral center A^0, transforming it to an A^- center by investing the energy $H^{(\beta)}(-/0)$ [Eq. (3)]. If all three species A^0, A^+, and A^- involve the same space orbital $\alpha=\beta$ in the electron-transfer processes, then we have the diagonal Mott-Hubbard energy for A^0, given by the difference in single-donor and single-acceptor energies (referred to the same band edge) as

$$U^{\alpha\alpha}(A^0)=E^{(\alpha)}(0/+)+[H^{(\alpha)}(-/0)-E_g] . \quad (10)$$

For most impurities, $U^{\alpha\alpha}(A^0)$ is positive; i.e., the donor level is lower in the gap than the acceptor level if the two transitions are associated with the same center. A different apparent Mott-Hubbard energy can be obtained for the A^- center by first removing an electron from orbital α on A^-, transforming the center to A^0 through an energy change $H^{(\alpha)}(-/0)$ [Eq. (3)], and then adding an electron to orbital β of an A^- center, transforming it to an A^{2-} center through an energy change $E^{(\alpha)}(-/2-)$ [Eq. (6)]. The diagonal Mott-Hubbard energy for A^- is given by the difference in double-acceptor and single-acceptor energy as

$$U^{(\alpha\alpha)}(A^-)=E^{(\alpha)}(-/2-)-E^{(\alpha)}(0/-) , \quad (11)$$

where we have referred both acceptor energies to the valence-band edge. For most impurities, $U^{(\alpha\alpha)}(A^-)$ is

positive too; i.e., the single-acceptor level is lower in the gap than the double-acceptor level if both belong to the same center.

Experimental values for these Mott-Hubbard energies are given in Figs. 1(a)–5(a). They are $U^{(tt)}(A^-)=0.73$ and 1.05 eV for GaP:Cr and GaP:Ni, respectively; $U^{(ee)}(A^0)=1.39$ eV for GaP:Fe, and $U^{(tt)}(A^0)=(0.62\pm0.1)$ eV for GaP:Cr. Within experimental error, $U^{(\alpha\alpha)}(A^-)\cong U^{(\alpha\alpha)}(A^0)$ for GaP:Cr (the only impurity in this series for which a donor has been observed). For sp-electron impurities (e.g., GaP:S, GaP:Si, GaP:Ge), one could guess from the knowledge of the valence difference ΔZ between the impurity and the host atom it replaced whether the system will show donor or acceptor action. However, the larger U values for GaP:TA make such predictions impossible. For example, while GaP:Fe has excess electrons in its highest-energy orbital available for donation, upon removal of one such electron the level moves downward by $U^{(ee)}$ and disappears into the valence band. Hence, GaP:Fe shows no donor action. We will see in Sec. VI how mean-field one-electron effects as well as multiplet effects combine to give this result.

D. General properties of these transitions

A few remarks are in order for clarifying the nature of these ionization processes. First, whereas the crystal as a whole conserves its charge both in acceptor [Eqs. (2) and (4)] and in donor [Eq. (7)] ionizations, the impurity subspace changes its formal charge. This implies a change in the *orbital occupation space*, but it does not imply necessarily that the *impurity site* changes its charge by an integer number in coordinate space. Historically,[63,64] the notation of formal charge states, A^+, A^0, A^-, etc., has often identified the formal charge with a physical (ionic-like) charge that resides on the impurity atom. No such implication is made here (cf. Sec. VI D).[59,62] Second, the charge in free energies $H(-/0)$, $E(-/2-)$, and $E(0/+)$ does not equal the change in the ground-state orbital energies, but rather a change in the *total energy* of the final and initial system, each evaluated at its equilibrium geometry pertinent to the experimental conditions. Changes in the electrostatic (Madelung) energies as well as in lattice relaxations can contribute to these ionization energies. In an equilibrium experiment (e.g., DLTS, Hall effect) this means that both initial and final states can take up relaxed equilibrium geometries, whereas in nonequilibrium experiments (e.g., photoabsorption) this may not be so. Third, the sum of the energy for (acceptor) hole emission [Eq. (2)] and (acceptor) electron capture [Eq. (4)] need not equal the band-gap energy, since different electronic and structural relaxations can be involved in each case. In practice, however, in the few cases where both transitions have been measured (reviewed in Ref. 52) the sum is indeed very close to the band-gap energy, suggesting small (or similar) relaxation energies in both processes. The same is true for (donor) electron emission [Eq. (7)] and (donor) hole capture [Eq. (9)]. We will hence consider only one member of each complementary pair, i.e., acceptor hole emission [Eqs. (2) and (3)] and donor electron emission [Eqs. (7) and (8)]. Finally, the expressions in

Eqs. (1)—(9) for the various transitions denote explicitly only the levels e and t that undergo an occupation change. This does not imply, however, that the corresponding transition energies depend only on these (gap) levels. For transition-atom impurities in ionic host crystals[63,64] it is often assumed that the e and t levels have only a weak electronic coupling to the host crystal (since all $3d$ orbitals appear as gap levels) and only they are involved in the excitation. This is not the case for transition-atom impurities in covalent systems.[53,54] There, in addition to the gap levels, part of the $3d$ intensity appears as valence-band resonances. Hence, when the e and t gap levels are altered in *occupation space* through excitation, the valence-band resonances undergo changes in *coordinate space* (i.e., their degree of spatial localization changes when the "outer" gap levels are excited.) We mean by our notation in Eqs. (1)—(9) that the change in total energy upon excitation includes both the (explicit) contributions of the e and t "outer" gap levels as well as the (implicit) contribution from the rearranged valence-band resonances. In our calculation of the mean-field part of the excitation energies (Secs. IV D and V) we will treat the impurity and its host crystal self-consistently as a whole, evaluating the changes in the total energies and letting both the gap orbitals as well as the valence-band resonance orbitals relax.

IV. MANY-ELECTRON VERSUS ONE-ELECTRON (MEAN-FIELD) CONTENT OF TRANSITION ENERGIES

A. General discussion

In general, the excitation and ionization energies observed experimentally [Figs. 1(a)—(5a)] and formulated in Eqs. (1)—(9) could arise both from many-electron (multiplet) effects as well as from one-electron (mean-field) contributions. The relative importance of these two contributions has been a subject of controversy in the context of band theory of perfect solids[55] as well as in the theory of point defects.[65] This situation is well known in the physics of Mott insulators[55,56] (e.g., MnO, CoO, and NiO), where spin-restricted one-electron band theory usually predicts such systems to be partially filled d-band metals at least above the Néel temperature (e.g., CoO) or narrow-gap semiconductors (e.g., NiO and MnO), whereas, in fact, with the exception of VO and TiO, all $3d$ monoxides are wide-gap (Mott) insulators both above and below the Néel temperature. This failure of mean-field theory is ascribed in Mott's picture[67] to the neglect of space and spin many-electron correlation effects which lead to site-localized states. Indeed, when a $3d$ element is surrounded by highly electronegative narrow-band ligands such as oxygen, Mott's picture[67] suggests that the ground state involves "broken-symmetry" configurations where the metal states are atomically localized, retaining large Coulomb energies and local magnetic moments, and sustaining atomiclike multiplet excitations which have no place in one-electron band theory. At the other limit, when a $3d$ element is surrounded by ligands capable of sustaining itinerant covalent bonds such as silicon (e.g., TA silicides), the ground state of the system is often described successfully[68] by itinerant band theory, showing,

in agreement with experiment, covalent metallic bonding, weak or no magnetism, and a normal band-to-band excitation spectrum. Between these limits we find the transition-metal phosphides and arsenides ($3d$ pnictides[69]), which exhibit mixed characteristics, appearing both as insulators and as metals, having more complex crystal structures [e.g., the hexagonal NiAs-type ($B8_1$) structure, or the orthorombic MnP-type ($B31$) structure] and magnetic properties. Transition-atom impurities in GaP constitute the "dilute limit" of such bulk pnictides. The extent of many-electron multiplet effects in such systems is not obvious *a priori*. A similar transition between the prevalence of one-electron effects to the dominance of localization with its attendant many-electron effects is familiar in spectroscopy of covalent semiconductors and insulators.[59(d)] Whereas the general features of the low-energy electronic excitations (interband spectra) could be described reasonably well by itinerant band theory, the higher-energy excitations in the same systems, involving core holes and core excitons,[59(d)] are often dominated by many-electron multiplet phenomena. Again, the GaP:TA system forms an intermediate case, as its spectra involve excitations of localized "semi-core-like" $3d$ orbitals in a semiconducting matrix.

Spin- and space-restricted electronic structure calculations of both bulk solids and point impurities have traditionally made strong commitments to the one-electron viewpoint of such systems. This commitment is rooted in the fundamental computational strategy chosen. Largely because of computational ease, the spin- and space-restricted (hereafter referred to as mean-field, or MF) calculations of systems with incomplete one-electron levels restrict the one-particle charge density to have the symmetry of the underlying nuclear framework (i.e., to belong to the totally symmetric a_1 representation of the physical symmetry group). This means that if n electrons are available for occupying a degenerate level that can accommodate a larger number, N, of electrons, one constructs the one-particle charge density using a procedure equivalent to assigning n/N electrons to each of the N partners. For example, in the d^3 configuration, one assigns $3/10$ electrons to each of the 10 degenerate partners of the d level. By Unsöld's theorem the density constructed in this way is totally symmetric. This procedure, common to many contemporary calculations of atoms,[70] bulk metals,[71] and impurities,[59-62] constitutes an enormous computational simplification, since all different arrangements of electrons being explored share the same simplest form of a highly symmetric one-particle density and potential. However, this symmetrization also deprives the system of much of the spatial correlation energy since it does not allow different electron orbits to get out of each other's way by occupying spatially distinct and variationally independent orbitals. (The spin part of this correlation energy can be represented approximately by spin-polarized calculations, e.g., as in Fig. 6.) The piece of the charge density that is omitted from mean-field calculations (i.g., the non-totally-symmetric density) is responsible for two major effects in impurity physics: the Jahn-Teller (JT) distortion and the multiplet splitting. Mean-field calculations, however, do not provide direct informa-

tion on the magnitude or importance of many-electron effects, except in an *a posteriori* fashion when the success or failure in reproducing the experiment is analyzed. Direct calculation of many-electron energies from the self-consistent Green's-function wave functions appears prohibitively complex and has not been attempted yet for any system. Hence, before undertaking the task of performing electronic structure calculations on $3d$ impurities, the relative significance of many-electron versus one-electron effects needs to be assessed. We will do this along the conceptual framework similar to that suggested by Allen.[72]

B. Separation of the observed transition energies into mean-field and multiplet contributions

In a recent work, Fazzio, Caldas, and Zunger[52] (FCZ) constructed an approximate method for deconvoluting the observed excitation and ionization energies of Eqs. (1)—(11) into a piece that derives from mean-field (MF) effects and a piece due to multiplet corrections (MC). Specifically, the intracenter excitation energy $\Delta^{(ij)}[e^m t^n; e^{m'} t^{n'}]$ of Eq. (1) is formulated as

$$\Delta^{(ij)}[e^m t^n; e^{m'} t^{n'}] = \Delta_{\text{eff}}[e^m t^n; e^{m'} t^{n'}] + (E_{\text{MC}}^{(j)} - E_{\text{MC}}^{(i)})$$

$$\equiv \Delta_{\text{eff}}[e^m t^n; e^{m'} t^{n'}] + \Delta E_{\text{MC}}^{(ij)} . \quad (12)$$

Here, the first term, $\Delta_{\text{eff}}[e^m t^n; e^{m'} t^{n'}]$ (the "effective crystal-field splitting"), is the *mean-field* total-energy difference that separates the two one-electron configurations:

$$\Delta_{\text{eff}}[e^m t^n; e^{m'} t^{n'}] = E_{T,\text{MF}}[e^{m'} t^{n'}] - E_{T,\text{MF}}[e^m t^n] . \quad (13)$$

The effective crystal-field energy Δ_{eff} differs from the classic crystal-field splitting used in the Tanabe-Sugano (TS) model.[64] It includes (i) bare-ion contributions, (ii) covalency effects (i.e., screening by the impurity's electrons), and (iii) *average* multiplet effects. All are incorporated in mean-field calculations like ours (e.g., that of Refs. 58—62); the last two are absent (at least formally) in the classical TS approach. The second term in Eq. (12) includes multiplet corrections, where $E_{\text{MC}}^{(j)}[e^{m'} t^{n'}]$ and $E_{\text{MC}}^{(i)}[e^m t^n]$ are, respectively, the energy of multiplet $|j\rangle$ derived form the predominant one-electron configuration $e^{m'} t^{n'}$ and the energy of multiplet $|i\rangle$ derived from $e^m t^n$, both measured relative to the respective *multiplet average energies*. Similarly, for the ionization process of Eqs. (3), (8), and (6), the deconvolution is formulated, respectively, as

$$H_{ij}^{(\alpha)}(-/0) = H_{\text{MF}}^{(\alpha)}(-/0) + [E_{\text{MC}}^{(j)}(A^-) - E_{\text{MC}}^{(i)}(A^-)]$$

$$\equiv H_{\text{MF}}^{(\alpha)}(-/0) + \Delta H_{\text{MC}}^{(ij)}(-/0) , \quad (14)$$

$$E_{ik}^{(\alpha)}(0/+) = E_{\text{MF}}^{(\alpha)}(0/+) + [E_{\text{MC}}^{(k)}(A^+) - E_{\text{MC}}^{(i)}(A^0)]$$

$$\equiv E_{\text{MF}}^{(\alpha)}(0/+) + \Delta E_{\text{MC}}^{(ik)}(0/+) , \quad (15)$$

$$E_{jl}^{(\alpha)}(-/2-) = E_{\text{MF}}^{(\alpha)}(-/2-) + [E_{\text{MC}}^{(l)}(A^{2-}) - E_{\text{MC}}^{(j)}(A^-)]$$

$$\equiv E_{\text{MF}}^{(\alpha)}(-/2-) + \Delta E_{\text{MC}}^{(jl)}(-/2-) . \quad (16)$$

Here, $H_{\text{MF}}^{(\alpha)}(-/0)$, $E_{\text{MF}}^{(\alpha)}(0/+)$, and $E_{\text{MF}}^{(\alpha)}(-/2-)$ are the differences in *mean-field* total energies pertinent to a single acceptor, single donor, and double acceptor, respec-

tively, i.e., they have analogous expressions to Eqs. (3), (8), and (6), respectively, except that the many-electron total energy E_T is replaced by the mean-field total energy $E_{T,\text{MF}}$. The correction terms due to many-electron multiplet effects are given in square brackets in Eqs. (14)—(16). Here, $E_{\text{MC}}^{(i)}(A^0)$, $E_{\text{MC}}^{(j)}(A^-)$, $E_{\text{MC}}^{(k)}(A^+)$, and $E_{\text{MC}}^{(l)}(A^{2-})$ are the many-electron shifts of the ground-state multiplets $|i\rangle$, $|j\rangle$, $|k\rangle$, and $|l\rangle$, respectively, of the species A^0, A^-, A^+, and A^{2-}, respectively.

The apparent Mott-Hubbard[67] Coulomb repulsion energies of Eqs. (10) and (11) can be deconvoluted similarly, yielding

$$U_{ijk}^{(\alpha\alpha)}(A^0) = U_{\text{MF}}^{(\alpha\alpha)}(A^0) + [\Delta E_{\text{MC}}^{(ik)}(0/+)$$

$$+ \Delta H_{\text{MC}}^{(ij)}(-/0)]$$

$$\equiv U_{\text{MF}}^{(\alpha\alpha)}(A^0) + \Delta U_{ijk}^{(\alpha\alpha)}(A^0) \quad (17)$$

and

$$U_{ijl}^{(\alpha\alpha)}(A^-) = U_{\text{MF}}^{(\alpha\alpha)}(A^-) + [\Delta E_{\text{MC}}^{(jk)}(-/2-)$$

$$+ \Delta H_{\text{MC}}^{(ij)}(-/0)]$$

$$\equiv U_{\text{MF}}^{(\alpha\alpha)}(A^-) + \Delta U_{ijl}^{(\alpha\alpha)}(A^-) . \quad (18)$$

Here, $U_{\text{MF}}^{(\alpha\alpha)}(A^0)$ and $U_{\text{MF}}^{(\alpha\alpha)}(A^-)$ are the *mean-field* Coulomb energies and $\Delta U_{ijk}^{(\alpha\alpha)}(A^0)$ and $\Delta U_{ijl}^{(\alpha\alpha)}(A^-)$ are the corresponding *multiplet corrections*.

Next, one has to evaluate the magnitude of the many-electron correction terms in Eqs. (12)—(18). In the theory of FCZ, the multiplet correction terms can be obtained in terms of the known[63] free-ion Racah parameters B_0 and C_0 of the free impurity ions and in terms of three physical parameters characterizing each impurity-host system. These are the orbital deformation parameters λ_e and λ_t of the impurity Wannier orbitals of type e and t, respectively, and the effective crystal-field splitting Δ_{eff} of Eq. (13). In the limit of atomically localized impurity states, the orbital deformation parameters (measuring the strength of interelectronic interactions in the solid relative to the free ion) approach unity, whereas in the opposite limit of completely delocalized impurity states they diminish to zero. In principle, λ_e and, λ_t could be calculated from mean-field theory by constructing the impurity Wannier orbitals (in the sense of Kohn and Onffroy[73]) using both the gap level and the occupied resonance wave functions. Together with Δ_{eff} of Eq. (13) these could be used to calculate the multiplet structure of each charge state and hence the multiplet corrections in Eqs. (14)—(18). Such a frontal attack on the calculation of ΔE_{MC} from the electronic structure of the impurity was deemed to be intractable (see, however, Sec. VI A 2). FCZ have taken the alternative approach, evaluating the magnitude of the multiplet corrections underlying the *experimental data themselves;* i.e. deconvoluting the observed transition energies into a MF and a MC, using their multiplet theory with its parameters, as an intermediate step. To this end, they fitted the observed intracenter $A^- \rightarrow (A^-)^*$ excitation spectra, obtaining λ_e, λ_t, and Δ_{eff} directly from experiment. Owing to the scarcity of data, a single Δ_{eff} value was used and spin-orbit corrections (which introduce more parameters) were neglected. When the number of observed transitions

was smaller than the number of parameters, a range of these parameters, consistent with the data, was determined. The interested reader is referred to Ref. 52 for a complete description of the details of the method. We next apply this method to GaP:TA and discuss the content of this deconvolution.

C. Analysis of the experimental data for GaP:TA

The chemical trends obtained for λ_e, λ_t, and Δ_{eff} for all $3d$ impurities for which data exist in ZnO, ZnS, ZnSe, and GaP, as well as for the Mott insulators[66] MnO, CoO, and NiO, were described previously.[52] Using these experimentally deduced mean-field parameters, one can calculate the full multiplet structure of the ground and excited states of A^0, A^+, A^-, and A^{2-} centers, establishing also the predominant one-electron configuration $e^m t^n$ in each multiplet. The Appendix gives the details of the fit for GaP:TA and the resulting mean-field parameters. Figures 1(a)—5(a) show the assignments of multiplets and the corresponding one-electron configurations for all excitation and ionization processes observed in GaP:TA. In all cases where ESR or ENDOR data were available (Appendix), we find that the total spin J obtained in our calculations agrees with experiment, cf. Figs. 1(a)—5(a). Having obtained in this way the multiplet structure, it is further possible to evaluate the multiplet *correction* $\Delta E_{MC}^{(ij)}$ for excitations [Eq. (12)], the corrections $\Delta H_{MC}^{(ij)}(-/0)$, $\Delta E_{MC}^{(ik)}(0/+)$, and $\Delta E_{MC}^{(jl)}(-/2-)$ for single-acceptor, single-donor, and double-acceptor ionizations [Eqs. (14), (15), and (16), respectively], as well as the multiplet corrections $\Delta U_{ijk}^{(\alpha\alpha)}(A^0)$ and $\Delta U_{ijl}^{(\alpha\alpha)}(A^-)$ for the Mott-Hubbard Coulomb energies [Eqs. (17) and (18), respectively].

The content of this deconvolution is revealing. This is illustrated in Fig. 7, which displays the MF portion (shaded area) and the MC part (clear area) of the single-acceptor energies [Fig. 7(a) and Eq. (14)], double-acceptor energies [Fig. 7(b) and Eq. (16)], and the lowest $d \rightarrow d^*$ intracenter excitation energies [Fig. 7(c) and Eq. (12)]. The solid circles represent the sum $\Delta E_{MF} + \Delta E_{MC}$. The simple chemical trends obtained in the mean-field parameters λ_e, λ_t, and Δ_{eff} deduced from experiments[52] are seen to transform into a more complex trend in the many-electron energies. First, on the physically relevant energy scale of the host-crystal band gap ($E_g = 2.35$ eV), the many-electron corrections are seen to constitute a significant portion of the ionization energies, and consequently could not be ignored. The qualitative trends observed parallel the Lewis generalized acid-base formulation of acceptors and donors,[74] e.g., Mn has a large MC for its first-acceptor transition and Cr has a large MC for its double-acceptor transition, since both systems attempt to complete their $d^4(e^2 t^2)$ configuration to the stabler, half-filled configuration $d^5(e^2 t^3)$, etc. This is, in part, the reason why in the series of first-acceptor energies there is a maximum at Fe($d^5 \rightarrow d^6$) and minimum at Mn($d^4 \rightarrow d^5$), whereas in the series of double acceptors we predict a minimum at Cr($d^4 \rightarrow d^5$) and a maximum at Mn($d^5 \rightarrow d^6$) (however, these double-acceptor energies are predicted to reside just above the CBM). Second, note that the MC can be either negative (e.g., single acceptors in GaP:Cr
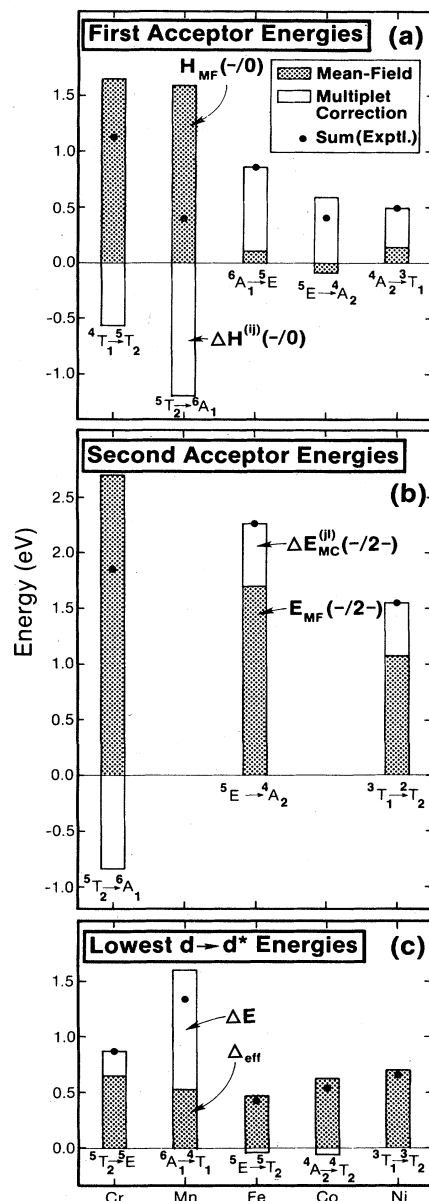

FIG. 7. Deconvolution of the experimental transition energies for (a) single acceptors, (b) double acceptors, and (c) intracenter $d \rightarrow d^*$ excitation energies for TA impurities in GaP into a mean-field contribution (shaded area) and many-electron multiplet corrections (clear area). The solid circles denote their sum (i.e., the experimentally observed energies).

and GaP:Mn, double acceptor in GaP:Cr), or positive (e.g., single and double acceptors in GaP:Fe and GaP:Ni). When the transition involves an increase in spin (e.g., the $^4T_1 \rightarrow {}^5T_2$ first acceptor in GaP:Cr), the MC is negative, whereas when the transition involves a reduction in spin (e.g., the $^6A_1 \rightarrow {}^5E$ first acceptor in GaP:Mn), the MC is positive. This mimics the expectations from spin-polarization effects. However, even spin-conserving transitions (for which there are no contributions from spin polarization in free ions) are seen to have either small positive (the $^5T_2 \rightarrow {}^5E$ intracenter excitation in GaP:Cr), or

small negative (e.g., the $^5E \rightarrow {}^5T_2$ intracenter excitation in GaP:Fe), multiplet corrections. Third, note that the MF portion of the transition energy is positive, with only one exception (the first acceptor in GaP:Co). Finally, note that by Eqs. (17) and (18), and (12), the results of Fig. 7 imply also that the apparent Mott-Hubbard Coulomb energies and the crystal-field energies have both a mean-field component and a multiplet correction component. Taking the corresponding differences between Figs. 7(b) and 7(a), for example, we find that for GaP:Cr, GaP:Fe, and GaP:Ni the mean-field contributions $U_{MF}(A^-)$ [Eq. (18)] are 1.04, 1.60, and 1.29 eV, respectively, whereas the multiplet correction parts $\Delta U(A^-)$ [Eq. (18)] are -0.31, -0.21, and -0.25 eV, respectively. Multiplet effects are seen here to reduce $U^{(\alpha\alpha)}$ relative to $U_{MF}^{(\alpha\alpha)}$. One can hence imagine a situation[52] where lattice-relaxation effects alone cannot produce a negative value for U, but, when combined with multiplet effects, one can have $U < 0$, i.e., a donor level above the acceptor level.

Considering the multiplet corrections to the *ground state* of A^0 and A^-, we find them to be less than 1 eV at both the Cr and the Ni ends of the $3d$ series, but larger (1.5–3 eV) at the center of the $3d$ series. Since these corrections are proportional to spin-polarization energies,[52] and since Jahn-Teller distortions and spin polarization are competing effects, this suggests that Cr and Ni are more likely to undergo a JT distortion than other impurities with degenerate ground states but larger correlation energies. Indeed, so far only Cr and Ni were observed to undergo substantial distortions (Appendix). In more ionic host crystals (e.g., ZnS; cf. Ref. 52), the ground-state multiplet stabilization energies are larger ($\lesssim 4$ eV) than in GaP.

The orbital deformation parameters λ_e and λ_t (given in the Appendix) are reduced in the covalent solid to 0.7–0.8, compared with their values in oxides[66] (~ 0.9) and free ions (1.0). We see, however, that, whereas this reduction is sufficient to attenuate significantly the *magnitude* of ionization and excitation energies relative to the free ions,[59(c)] it still leaves a significant *proportion* of many-electron multiplet corrections in the transition energies. The existence of such a substantial proportion of many-electron contributions (even larger[52] for ZnS:TA and ZnSe:TA) suggests to us that, whereas electronic structure models with a number of *ad hoc* parameters[19,36] or with numerous adjustable parameters[53(b)] may simulate experiments, a first-principles mean-field calculation could not legitimately come close to experiment. Indeed, only large-scale, multiconfiguration self-consistent-field (MCSCF) models, or self-interaction-corrected, spin-polarized calculations[75,76] could hope to achieve this goal. Instead, we propose to use a first-principles mean-field theory and compare the results with the mean-field part of the experimental data (shaded areas in Fig. 7). A simple scheme that facilitates such a comparison is described in the next subsection.

### D. Energy-level diagrams for the mean-field transitions

The transition energies $H_{MF}(-/0)$, $E_{MF}(0/+)$, $E_{MF}(-/2-)$, and Δ_{eff}, and the Coulomb energy U_{MF},

correspond to a total-energy difference, and hence they could not be readily displayed in terms of one-electron-like energy-level diagrams. A practical disadvantage of expressing transition energies as differences in total energies lies in the fact that each total energy in Eqs. (13)–(16) contains a large, common term (the ground-state energy of the host crystal), but only a rather small difference (change in $E_{T,MF}$ upon changing the occupation numbers of two levels) is of interest. However, having identified the particular configuration changes $e^m t^n \rightarrow e^{m'} e^{n'}$ attendant upon the relevant transitions [Figs. 1(a)–5(a)], one could construct approximate mean-field energy-level diagrams (as opposed to the quasiparticle diagrams of Sec. VI C) using Slater's transition-state concept.[77] Correct to second order, the difference in total energies attendant upon a configuration change $V^Q t^m \rightarrow V^{Q'} t^{m'}$ is given by the difference in the corresponding self-consistent density-functional orbital energies, computed at the intermediate occupation numbers $(Q + Q')/2$ and $(m + m')/2$:

$$E_T[V^{Q'} t^{m'}] - E_T[V^Q t^m] \cong [\epsilon_V - \epsilon_t]_{V^{(Q+Q')/2} t^{(m+m')/2}} . \quad (19)$$

This transition-state approach has been applied extensively to transition atoms reproducing the difference in total energies for $3d$ excitations to within $\gtrsim 0.1$ eV. Some of the properties of this approximation are (i) the right-hand side of Eq. (19) is meaningful only for a given geometry of the impurity system, (ii) it includes approximately the effect of electronic relaxation, (iii) it incorporates not only the direct contributions of the levels V and t but also the indirect (screening) effects of all other levels included in the self-consistent calculation (e.g., valence-band resonances), and (iv) it incorporates the lowest-order effects of the self-interaction correction.[76] Because of (i) above, our strategy will be as follows. We will calculate ΔE_{MF} by performing separate self-consistent QBCF calculations for each transition-state configuration pertinent to the various donor and acceptor transitions. We will assume throughout the calculation the unrelaxed geometry of the ideal crystal. We will then compare our results for ΔE_{MF} with the experimentally deduced mean-field energies $\Delta E - \Delta E_{MC}$. The discrepancies with experiments, where they exist, will reflect a combination of the amount by which the transition-state local-density model fails to be a perfect MF theory, and the *change* in lattice distortions attendant upon the particular transition, which has been left out. (In a single instance, i.e., the e level of GaP:Co, cf. Fig. 8, we find a partially occupied level inside the valence band. The discrete representation used in the QBCF method allows us, nevertheless, to identify unambiguously this highly localized state and define its occupancy throughout the self-consistency iterations.)

The mean-field excitation and ionization energies deduced from experiment are depicted in Fig. 1(b)–5(b), together with the corresponding transition-state occupation numbers. For example, the total-energy difference attendant upon the first-acceptor transition in Ga:Cr [$(-/0)$ in Fig. 1(a)], i.e.,

$$[A^0, Cr^{3+}, {}^4T_1(e^2 t^1)] \rightarrow [A^-, Cr^{2+}, {}^5T_2(e^2 t^2)] ,$$
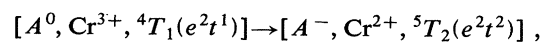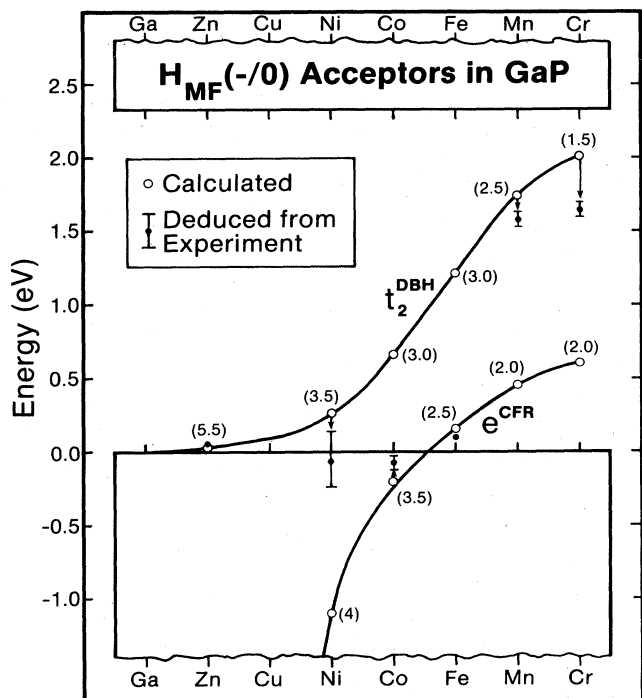
FIG. 8. Calculated near-gap impurity-induced energy levels (open circles), compared with the mean-field values for first acceptors deduced from experiment (solid circles). Arrows connect the corresponding levels, to guide the eye. Numbers in parentheses indicate the (transition-state) occupation numbers pertinent to a first-acceptor transitions. The result for GaP:Cu is an interpolation.

is represented within the mean-field transition-state approximation [(−/0) MF in Fig. 1(b)] as the energy separation between the t level and the top of the valence band, using the intermediate $(VB)^{5.5}e^2t^{1.5}$ configuration for the self-consistent calculation [Fig. 1(b)]. The first-donor transition,

$$[A^0, Cr^{3+}, {}^4T_1(e^2t^1)] \rightarrow [A^+, Cr^{4+}, {}^3A_2(e^2t^0)]$$
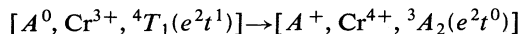
[Fig. 1(a)], likewise has a MF contribution represented by the energy separation between the conduction-band minimum and the t level, using the intermediate $(CB)^{0.5}e^2t^{0.5}$ configuration. The Mott-Hubbard Coulomb energy $U_{MF}^{(tt)}(A^0)$ for the A^0 center is then given by the separation of the two t-level energies in the acceptor and donor calculations [Fig. 1(b)]. The intracenter excitation of the A^- center,

$$[A^-, Cr^{2+}, {}^5T_2(e^2t^2)] \rightarrow [(A^-)^*, Cr^{2+}, {}^5E(e^1t^3)]$$
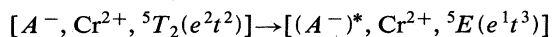
[Fig. 1(a)], is represented by the difference in t and e-orbital energies, using the intermediate configuration $e^{1.5}t^{2.5}$ [Fig. 1(b)]. Figures 1(b)—5(b) display the relevant transition-state configurations for all transitions in Cr, Mn, Fe, Co, and Ni in GaP, and give the mean-field values for the transition energies, as obtained from the analysis of the experimental data. Owing to its ultrafast diffusivity, Cu tends to form complexes which obscure the data for the isolated substitutional impurity. It is

hence not discussed here.

Notice that inherent limitations[76] in the restricted local-density version[78] of the general density-functional formalism[79] prevent the theory from predicting, in general, the correct many-electron ground-state configuration. Recognizing these limitations, we do not attempt to predict in this work the one-electron configurations that correspond to the transitions in Figs. 1—5, but instead we have deduced these configurations from our analysis of the experimental data. (Recent spin-unrestricted calculations[75] for interstitial Si:Fe indicate that, when self-interaction corrections[76] are incorporated, the correct configurations are predicted.) Notice further that our analysis of the experimental data shows that mean-field calculations could legitimately show a partially empty level in resonance with the valence band [e.g., the e level of the first acceptor of GaP:Co in Fig. 4(b)], a seemingly "unphysical" situation that is nevertheless entirely consistent with the data once many-electron corrections are acknowledged. This simply means that, whereas a fully correlated ("exact") calculation will predict in a single step the correct many-electron ground state, and will presumably not show partially filled levels in resonance with the continum, if one chooses to proceed instead by adding correlation corrections to a manifestly imperfect correlationless (MF) calculation, it is entirely legitimate to expect different configurations, including partially filled resonances.[80]

We next proceed to describe the method used for the self-consistent mean-field calculation (Sec. V) and compare the results with the mean-field energies deduced from experiment (Sec. VI).

V. METHOD OF CALCULATION

We have used the self-consistent quasiband crystal-field Green's-function method[58,81] within the local-density formalism[78] to calculate the electronic structure of GaP:TA for TA=Zn, Ni, Co, Fe, Mn, and Cr. A limited number of calculations, pertaining to the neutral center, were also carried out for GaP:Cu, as well as for the limit GaP:Ga [Ref. 59(d) and below]. The same method had been previously used to study substitutional[59] and interstitial[62] $3d$ impurities in Si, the unrelaxed silicon vacancy,[58] substitutional and interstitial Cu, Ag, and Au impurities in Si [Ref. 59(e)] chalcogen (O, S, Se) impurities in silicon,[61,82] and core excitons in GaP.[59(d)] The method and its convergence properties were discussed previously in detail.[58,81] Here we will merely indicate the input parameters. In representing the electronic structure of GaP, we wanted to achieve physically correct (i) band structure, (ii) charge density, and (iii) equilibrium lattice constant. We have obtained the band structure of the GaP host crystal using a self-consistent plane-wave local-pseudopotential calculation. For the Ga and P pseudopotentials we have taken the nonlocal-density-functional potentials of Zunger and Cohen,[83] obtained a local approximation to them by averaging the s and p pseudopotentials, and smoothed them analytically near the origin to obtain a potential that converges rapidly in momentum space. Using this potential in a self-consistent calculation with an exchange coefficient $\alpha = 1$ and a basis consisting of 89 plane waves at Γ,

TABLE II. Comparison of the present local-pseudopotential band structure of GaP with the fitted results of the empirical pseudopotential method (EPM) of Chelikowsky and Cohen (Ref. 84), the recent nonempirical local-density calculation of Wood and Zunger (Ref. 88), and experiment (Refs. 85—87). All calculations pertain to the experimental zero-pressure lattice constant of 5.45 Å.

State	Present calculation	EPM	Expt.	"Best" local density
Γ_{1v}	-12.61	-12.99	-13.2^a	-12.30
Γ_{15v}	0.0	0.0	0.0	0.0
Γ_{1c}	2.93	2.88	2.89^b	1.89
Γ_{15c}	4.42	5.24	$5.19,^b$ 4.87	3.94
X_{1v}	-10.01	-9.46	$-9.6,^a$ -9.7^c	-9.50
X_{3v}	-6.48	-7.07	-6.9^c	-6.66
X_{5v}	-2.50	-2.73	-2.7^a	-2.58
X_{1c}	2.27	2.16		1.56
Δ_c	2.21		2.35^b	1.50
L_{1v}	-10.76	-10.60	-10.6^a	-10.38
L_{2v}	-6.32	-6.84	-6.9^a	-6.54
L_{3v}	-1.02	-1.10	$-1.2,^a$ -0.8^c	-1.06
L_{1c}	2.81	2.79		1.68
X_3-X_{1c}	0.42	0.55	0.355	0.21

[a]Reference 87.
[b]Reference 85.
[c]Reference 86.

we find the band energies given in Table II, where we compare them to the best fit of the observed data within an empirical nonlocal model potential,[84] experiment,[85—87] and the recent local-density calculation of Wood and Zunger.[88] (The latter calculation approaches closely the best that can be done within the present-day local-density formalism: it uses first-principles nonlocal pseudopotentials, the Ceperly correlation as obtained by Perdew and Zugner[54] and a large plane-wave basis set consisting of 459 basis functions, and the corresponding 3527 momentum components of the screening potential.) It is clear from Table II that the "best" local-density-functional calculation produces a band structure that deviates considerably from experiment, whereas the empirically adjusted (involving as the only disposable parameters the choice $\alpha=1$) calculation used here is in good agreement with experiment. The calculated equilibrium lattice constant of GaP, obtained with the pseudopotential used here (yielding the band energies given in the second column of Table II) was 5.36 Å, compared with the experimental value of 5.45 Å, and the recent pseudopotential calculation of Froyen and Cohen[89(b)] yielding 5.34 Å. In constructing the host-crystal potential we have also been careful to obtain a physically correct ground-state charge density. The maximum in the valence-electron density and the position of the maximum from the phosphorous site, measured in units of the Ga-P distance d, are 31 e/cell and $0.32d$, respectively, compared with the experimental results[90] of (35 ± 3) e/cell and $0.31d$, respectively (the empirical results of Chelikowsky and Cohen[84] yield a less peaked and more ionically polarized density, i.e., 26 e/cell and $0.36d$, respectively). In the Green's-function calculation we use 30 host-crystal bands for each **k** point, plus five quasibands[81] per **k** point, calculated for the orbitals of the appropriate impurity. The impurity-centered basis set consists of a combination of analytical quantum-defect orbitals[82,91] (i.e., solutions to the central potential of the form $b/r^2-a/r$, where a and b are optimized to $a=12.5$ a.u.$^{-1}$ and $b=1.0$ a.u.$^{-2}$) and numerical orbitals of the TA impurity obtained by an integration of the atomic local-density Schrödinger equation. We use $12s$, $11p$, $11d$, $10f$, and $10g$ radial analytic orbitals, and a single numerical $3d$ orbital; counting both radial and angular parts, we have $12s$, $33p$, $60d$, $70f$, and $90g$ orbitals, or a total of 260 orbitals per atom. The impurity is characterized by a nonlocal l-dependent density-functional pseudopotential.[83] An exchange parameter of $\alpha=1$ is used throughout the calculations. The potential and density perturbations were expanded in a Kubic harmonic series up to $l=8$; self-consistency in the potential is obtained to within a maximum error of 20 mRy in coordinate space, and an average error not exceeding 5 mRy. The only adjustment done in our calculation is, hence, the use of an exchange parameter $\alpha=1$. A further approximation is the use of an average $(s+p)$ local,[89(a)] rather than a nonlocal, pseudopotential for Ga and P. All reported calculations are performed at the observed lattice parameter of 5.45 Å. Numerous convergence tests (e.g., such as those published in Refs. 58 and 81) indicate that a conservative estimate of the internal precision of the calculation (i.e., for the assumed impurity and host pseudopotentials and the local-density form of screening) is better than ±0.15 eV for the orbital energies, and, more characteristically, ±0.10 eV. Since the accuracy of the calculation (e.g., comparing theory and experiment for the acceptor energies) turned out to be of the order of 0.4 eV or better (cf. Table III below), the numerical precision is sufficient for analyzing the discrepancies with experiment, when they exist, in terms of physical factors left out of the theory rather than numerical uncertainties.

VI. RESULTS

A. Near-band-gap levels

1. Donors, acceptors, and Coulomb energies

Figure 8 depicts the self-consistently calculated impurity-induced e and t_2 energy levels in the vicinity of the fundamental band gap, using the occupation number pertinent to the transition-state $H(-/0)$ first acceptors [Figs. 1(b)—5(b)]. Along with the calculated levels (open circles), we give the mean-field energies deduced from experiment (solid circles) and indicate the correspondence between experiment and theory by arrows to guide the eye. Similar to our study of $3d$ impurities in Si,[59] we find two types of impurity-induced levels in the gap: the upper t_2 dangling-bond hybrid (DBH) and a lower-energy crystal-field resonance (CFR) of type e. Whereas the t_2^{DBH} level is confined to the band-gap region, starting in GaP:Zn as a shallow acceptor at $E_v + 0.02$ eV and ending up in GaP:Cr as a deep acceptor at $E_v + 2.02$ eV, the e^{CFR} level exists as a valence-band resonance for TA = Ga, Zn, Cu, Ni, and Co, and emerges first into the band gap for GaP:Fe. Our analysis of the data shows that the first-acceptor transitions for the impurities Zn, Cu, Ni, Mn, and Cr involve the ionization of the t_2^{DBH} electron, whereas the acceptor states of Co and Fe involve ionization of the e^{CFR} electron [Figs. 1(b)—5(b)]. This switch between Ni and Co, or Fe and Mn, cannot be deduced without acknowledging many-electron effects. Comparing the calculated values and the experimentally deduced values (given here in parentheses) for the first-acceptor levels associated with the t_2^{DBH}, we find, for GaP:Zn, GaP:Ni, GaP:Mn, and GaP:Cr, the values 0.02 (0.07),[8] 0.26 (0.14 to -0.24), 1.74 (1.59), and 2.02 (1.65) eV, respectively. Notice that for the d^9 system GaP:Zn the multiplet correction for the first-acceptor state vanishes and hence the mean-field prediction should be directly comparable with experiment (after the small effective-mass binding energy ~ 0.05 eV (Ref. 8) is added to our central cell term of 0.02 eV, to correct in a rough way for electrostatic effects). For the acceptor levels associated with our analysis of the experimental data with the e^{CFR} level, we find the values -0.20 (-0.08) eV for

GaP:Co and 0.13 (0.10) eV for GaP:Fe. The agreement with experiment is seen to be good (Table III), except for GaP:Cr and possibly GaP:Ni (depending on the correctness of the two different experimental assignments discussed in the Appendix, subsection 5), for which the calculated positions of the t_2 levels are about 0.4 eV *too high*. Interestingly, the two impurities for which our (lattice unrelaxed) calculation shows the large discrepancy with experiment are also known to involve lattice relaxation. GaP:Cr is known to be distorted both in its A^0 and A^- states, and GaP:Ni is known to be distorted at least in its A^- state (see the Appendix). It is therefore tempting to associate at least part of the discrepancy between theory and experiment for these two impurities to lattice relaxations. Such relaxations are indeed expected to *lower* the position of the (antibonding) t_2^{DBH} levels; the magnitude of ≤ 0.4 eV energy lowering of such levels is consistent (e.g., for sp-electron impurities in silicon[92(a)] with a modest relaxation of a few percent.[92(b)])

It is obvious from Fig. 7(a) that the experimentally observed single-acceptor levels (solid circles) show a non-monotonic trend with the impurity's atomic number (e.g., Mn has a shallower acceptor level than Fe). At the same time, it is clear from Fig. 8 that the mean-field t_2^{DBH} and e^{CFR} levels have a purely monotonic trend with the impurity's atomic number. The two observations are consistent because of the following two reasons. First, the observed acceptor energies of Cr and Mn are associated with ionization of the t_2^{DBH} level, whereas the acceptor level of Fe is associated with the ionization of the e^{CFR} level (Fig. 8). This is a solid-state effect, absent from the free-ion ionization energies.[57] Second, the many-electron multiplet correction [Fig. 7(a)] for GaP:Mn is negative (making the acceptor energy *smaller* than the MF value), whereas the multiplet correction for GaP:Fe is positive (making the acceptor energy *larger* than the MF value). This effect exists also in the corresponding free ions,[57] although its magnitude is attenuated in the solid 5 times.

Turning next to double-acceptor states, the calculated positions of the corresponding t_2^{DBH} levels compared with the experimentally deduced values (given here in parentheses) are 1.26 (1.06 to 1.37) eV for GaP:Ni and 2.58 (2.69) eV for GaP:Cr, whereas the value for GaP:Fe, pertinent to an ionization of the e^{CFR} level, is 1.53 (1.70)

TABLE III. Calculated (calc) and experimentally deduced mean-field (MF) results [Figs. 1(a)—5(a) and the Appendix] first acceptor $H_{\text{MF}}(-/0)$, second acceptor $H_{\text{MF}}(-/2-)$, and Coulomb repulsion energies $U_{\text{MF}}(A^-)$, given in eV. For GaP:Ni we give two sets of MF results, deduced from the two inconsistent sets of experimental results (see Appendix).

Impurities	Ionized level	First acceptor		Second acceptor		Coulomb repulsion	
		$H_{\text{MF}}(-/0)$	$H_{\text{calc}}(-/0)$	$H_{\text{MF}}(-/2-)$	$H_{\text{calc}}(-/2-)$	$U_{\text{MF}}(A^-)$	$U_{\text{calc}}(A^-)$
Cr	t_2	$E_v + 1.65$	$E_v + 2.02$	$E_v + 2.69$	$E_v + 2.58$	1.04	0.56
Mn	t_2	$E_v + 1.59$	$E_v + 1.74$				
Fe	e	$E_v + 0.10$	$E_v + 0.13$	$E_v + 1.70$	$E_v + 1.53$	1.60	1.4
Co	e	$E_v - 0.08$	$E_v - 0.20$				
Ni	t_2	$\begin{cases} E_v + 0.14 \\ \\ E_v - 0.24 \end{cases}$	$E_v + 0.26$	$\begin{cases} E_v + 1.37 \\ \\ E_v + 1.06 \end{cases}$	$E_v + 1.26$	$\begin{cases} 1.23 \\ \\ 1.29 \end{cases}$	1.0
Cu	t_2		$E_v + 0.10$				
Zn	t_2	$E_v + 0.07$	$E_v + 0.02$				

eV. The Coulomb repulsion energies $U_{MF}^{(tt)}(A^-)$ are hence $1.26-0.26=1$ eV for GaP:Ni (experimentally deduced value is $1.23-1.29$ eV); $2.58-2.02=0.56$ eV for GaP:Cr (experimentally deduced value is 1.04 eV), and the $U_{MF}^{(ee)}(A^-)$ for GaP:Fe is $1.53-0.13=1.4$ eV (experimentally deduced value is 1.6 eV). Our calculated second-acceptor energies are hence within 0.2 eV from experiment and the calculated Coulomb repulsion energies are within $0.2-0.5$ eV from experiment, being always too small. This suggests that the A^- state (e.g., Cr^{2+}) is stabilized by lattice distortion more than the A^{2-} state is (e.g., Cr^{1+}). The largest discrepancy occurs for GaP:Cr (0.48 eV). Indeed, its A^- state is known to be distorted, whereas the A^{2-} state is a symmetric $^6A_1$ state [Fig. 1(a)] and hence not subject to JT distortion. In general, one expects indeed that polarization and electrostatic ion-ion interactions would lead to a larger induced energy lowering for the higher oxidation state (i.e., Cr^{2+} versus Cr^{1+}).

A few observations can be made. First, the calculated Coulomb repulsion energies in GaP:TA are about $2-4$ times larger than those calculated[59,62] for substitutional Si:TA, consistent with the lesser covalency of GaP. Second, the Coulomb energies for the e^{CFR} orbitals (1.4 eV in GaP:Fe) are larger than those for the t_2^{DBH} orbitals (1.0 and 0.85 eV for Ni and Cr, respectively), consistent with the higher localization of the former. Third, we find that the energy of the t_2^{DBH} orbital is linear, to within a good approximation (≤ 0.1 eV), with its occupation number, a result paralleled approximately by the experimentally deduced Coulomb energies for GaP:Cr [Fig. 1(a)]. Finally, we notice that the Coulomb energies calculated here for GaP:TA are about 20 times smaller than those calculated for the free TA ions (Ref. 52, Fig. 17, and Fig. 6 here). At first, this appears to be surprising since the corresponding impurity orbitals are rather localized, and hence "covalency" (i.e., delocalization and hybridization) effect alone could not explain such a large reduction in U (similarly, small U values are observed for sp-electron impurities;[61] however, this is understandable on the basis of their rather extended orbitals). This reduction in U for $3d$ impurities was found[59(c)] to be a result of a self-regulating response of the valence-band resonances to changes in the occupation number (hence charge state) in the "outer" gap levels. It is this reduction in interelectronic repulsions of the impurity ions that enables a few different charge states to coexist in a relatively narrow energy range (the band gap). Since the reduction factor for Si:TA($\times 100$, cf. Ref. 59) is even larger than that in GaP:TA, it is tempting to speculate that the reduction factor for the Fe "impurity" in the highly covalent Heme-like biological systems (hemoglobin, Cytochrome-C) would equal or even exceed that of the Si:TA system, explaining the ease of the Fe^{2+} and/or Fe^{3+} oxidation and/or reduction cycles in electron-transporting biological systems.[56]

Using the Coulomb repulsion energies of Table III, the multiplet corrections for the acceptor states of Fig. 7, and the transition-state energies of Fig. 8, one can further predict the approximate position of the hitherto unobserved second-acceptor states of GaP:Mn and GaP:Co. We find for GaP:Mn and GaP:Cr the second acceptor to be about 0.3 eV and 0.02 eV, respectively, above the conduction-band minimum (CBM), and for GaP:Co we predict it to be at $E_v + 2.4$ eV (i.e., just above the CBM). The double acceptor for Cr (and perhaps for Co too) may be forced into the gap by pressure. Regarding donor states, except for GaP:Cr, the only one that comes close to the band gap is GaP:Co, which we predict to occur just below the valence-band maximum (VBM).

2. Effective crystal-field splittings and intracenter excitations

We have not conducted a systematic set of calculations for the configurations appropriate for the calculation of Δ_{eff} of all impurities in GaP [these configurations differ from those needed in the calculation of the acceptor energies, cf. Figs. 1(b)—5(b)]. For GaP:Fe we have calculated the t_2^{DBH}-e^{CFR} separation for the A^- center [using the $e^{2.5}t^{3.5}$ configuration, cf. Fig. 3(b)] and find $\Delta_{eff}=0.87$ eV, significantly larger than the MF value of (0.45 ± 0.03) eV deduced from experiment. Indeed, crystal-field energies are notoriously difficult to calculate from first principles.[93]

Recently, Hemstreet[94] calculated for InP:Fe the crystal-field splitting for the e^2t^3 state (Fe^{3+}) and the e^3t^3 state (Fe^{2+}) using the muffin-tin multiple-scattering $X\alpha$ (MS$X\alpha$) cluster method with a central Fe impurity, a shell of four phosphorus atoms, and 12 hydrogen "terminators." He found values of 0.71 and 0.64 eV, respectively. In our own QBCF calculation for this system we use the configuration $e^{2.5}t^{3.5}$ appropriate for determining Δ_{eff}, and find $\Delta_{eff}=0.92$ eV. Hence, our calculation yields a larger Δ_{eff} value than that obtained by Hemstreet and, consequently, exhibits a larger discrepancy relative to experiment. We wondered[95] how this difference can be traced to the different computational models (a five-atom cluster with 12 hydrogen terminators and overlapping muffin-tin spheres[94] versus an extended host crystal with nonspherical potentials). Attempting to mimic the spherical approximation attendant upon the MS$X\alpha$ cluster calculation, we have repeated a QBCF calculation for InP:Fe, this time setting to zero the nonspherical potential terms inside a sphere of radius $d/2$ around Fe (d is the host bond length). Further, to mimic the finite-cluster effect (only the four phosphorus nearest neighbors of Fe were used in the MS$X\alpha$ cluster model), we have set the total potential past the distance $1.75d$ to a constant. We find in such a truncated QBCF calculation that the e^{CFR} level moves up in energy, reducing the t_2-e splitting (for e^3t^3) from 1.32 to 0.72 eV, close to Hemstreet's value. Having reduced the full QBCF calculation to the truncated-QBCF model in steps, we can analyze the origin of the reduction in Δ_{eff} in the MS$X\alpha$ calculation (or, equivalently, in the truncated-QBCF calculation). We find that the neglect of the nonspherical corrections inside the impurity sphere is responsible for a ~20% reduction in Δ_{eff}. Next, the removal of the second shell of neighbors deprives the e^{CFR} level (which has no σ bonds, except with the next-nearest neighbors) from much of its stability, pushing it up in energy toward the t_2^{DBH} level and reducing, thereby, Δ_{eff}. This effect is responsible for

about 80% of the discrepancy. We conclude that although the Δ_{eff} obtained in cluster calculations with spherical potentials and hydrogen terminators[94] can be close to the experimentally deduced mean-field values, the Δ_{eff} obtained in more general MF calculations are larger than the experimental values.

Our results for the diagonal ($U^{(\alpha\alpha)}$) and off-diagonal ($U^{(\alpha\beta)}$) Coulomb energies make it possible to assess the effect of the charge state on the effective crystal-field splitting Δ_{eff}. Suppose that the A^{+} center has a configuration $e^{m}t^{n-1}$, the A^{0} center has a configuration $e^{m}t^{n}$, and the A^{-} center has the configuration $e^{m}t^{n+1}$. If the crystal-field splitting for A^{0} is denoted $\Delta \equiv \Delta(e^{m}t^{n})$, then the splitting for A^{-} is approximately $\Delta + \frac{1}{2}(U^{(tt)} - U^{(ee)})$ and that for A^{+} is $\approx \Delta - \frac{1}{2}(U^{(tt)} - U^{(ee)})$. The reason for this is that as the occupation of the t orbital increases by unity, its energy goes up by $\approx \frac{1}{2}U^{(tt)}$ due to t-t Coulomb repulsion, whereas the e level goes up by $\sim \frac{1}{2}U^{(et)}$ (even though its occupation is fixed) due to extra screening of e electrons by t electrons. Finding that usually $U^{(tt)} < U^{(et)}$ (since the e orbital is more localized than the t orbital), we predict $\Delta_{\text{eff}}(A^{-}) < \Delta_{\text{eff}}(A^{0}) < \Delta_{\text{eff}}(A^{+})$, and that the slope of the line is nearly constant, at about 0.1–0.2 eV per charge state. We are unaware of experimental data to check this prediction.

The orbital localization parameters λ_{e} and λ_{t} could be calculated if one knew the ($3d$-projected) impurity Wannier orbitals. For impurity states that have both gap levels and valence-band resonances of the same type (e.g., the t_{2}^{DBH} and t_{2}^{CFR} levels of GaP:Ni), this is a difficult task. However, if for a given representation the impurity induces only localized gap levels and no valence-band resonances of the same symmetry (e.g., the e^{CFR} level of GaP:Mn and GaP:Cr, cf. Fig. 8), one could directly use these wave functions as obtained in our calculation as reasonable approximation to the Wannier orbitals.[73] O'Neill and Allen (private communication) have used our QBCF wave functions for GaP:Mn and calculated, by numerical integration, $\lambda_{e} = 0.86 \pm 0.01$, in excellent agreement with the experimentally deduced value (Ref. 52 and our Appendix) of 0.86 ± 0.08. (Unfortunately, such a comparison is not possible for λ_{t} since both the t_{2}^{DBH} and the Wannier-transformed t_{2}^{CFR} orbitals of GaP:Mn are needed. From the t_{2}^{DBH} wave function alone, O'Neill and Allen calculate 0.66 ± 0.01, suggesting that the t_{2}^{DBH} gap level is responsible for about 80% of λ_{t}, the remaining contributions coming from resonances.) This single comparison available to date between the calculated impurity wave functions and experiment appears very encouraging.

B. Overall trends in impurity-induced energy levels

Having established the relation between the calculated near-gap energy levels and the observed electronic transitions, we next turn to the structure of the calculated impurity-induced resonances, for which no experimental observations exist. Figure 9 shows those levels for TA = Ga through Cr. For the broad e and t_{2} valence-band resonances, we display graphically only their centers of gravity. Energy levels that belong to the same type of impurity level are connected by a line, to guide the eye.
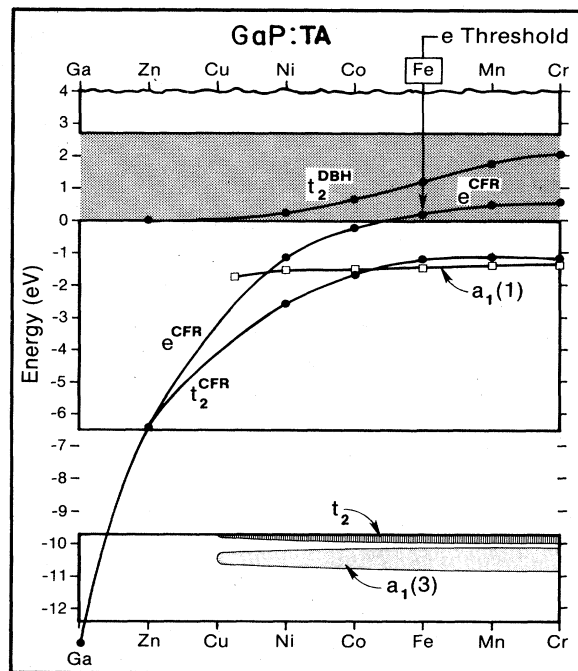

FIG. 9. Calculated impurity-induced energy levels in GaP:TA, using transition-state occupation numbers pertinent to first-acceptor states.

Except for GaP:Ga, the occupation numbers used pertain to the single acceptors and are hence identical to those used in Fig. 8.

1. e and t_2 crystal-field resonances

There is a striking resemblance between the levels of GaP:TA and those of substitutional TA impurities in silicon [Fig. 9 in Ref. 59(a)]. To understand the atomic origin of the impurity-induced levels, we place at the origin of Fig. 9 the trivial case of GaP:Ga, and continue to lighter impurities along the abscissa, hence going backward in the $3d$ series. The "impurity-induced" d levels of GaP:Ga are essentially the well-known Ga $3d$ bands in the pure GaP crystal. Clearly, because of the periodicity of the lattice, these "impurity-induced" states are broadened into bands. Nevertheless, the compactness (on the scale of the lattice constant) of the $3d^{10}$ orbitals of Ga makes this band extremely narrow.[59(d),96] These states can be represented either as the center of gravity of this narrow Ga $3d$ band, as obtained in band-structure calculations,[59(d),96] or, in complete analogy with our calculations for the other impurities, by replacing a single Ga host atom (described by a local pseudopotential, hence having no d bands) by a Ga atom described, like other TA impurities, by a nonlocal pseudopotential (hence, sustaining Ga $3d$ states). Using the latter procedure, we find[59(d)] (Fig. 9) the position of the Ga $3d$ levels in GaP in the absence of Ga $3d$—Ga $3d$ resonance interactions. (Since these are small, one obtains virtually the same result using either procedure.) As can be seen in Fig. 9, the Ga $3d$ or-

bitals in GaP appear as sharp states below the valence-band minimum. Since this "impurity" has a large (50 at. %) stoichiometric concentration, its ionization energy can be determined experimentally by x-ray photoelectron spectroscopy (XPS). The relation between this energy $[E_v - 18.5$ eV (Ref. 87)] and the position ($E_v - 13.1$ eV) of the one-electron $3d^{10}$ level given in Fig. 9 (involving a ~ 5-eV relaxation energy) was discussed elsewhere.[5(d)] The purpose of choosing GaP:Ga as the impurity at the origin of Fig. 9 and then proceeding to lighter impurities, going backwards in the Periodic Table, is to emphasize that the levels of GaP:TA for TA$\neq$Ga evolve naturally from the trivial case of GaP:Ga. For GaP:Ga we have the deep t_2 (or Γ_{25} in band-theory language) and e (or Γ_{12}) spin-unpolarized bands, fully occupied by six and four electrons, respectively, with a vanishingly small (crystal-field) splitting between them. As we replace the Ga impurity by Zn, with its weaker atomic Coulomb potential, the e^{CFR} and t_2^{CFR} levels have smaller binding energies, moving up to $E_v - 6.4$ eV (Fig. 9). As we proceed to Cu, Ni, etc., the $3d$ orbitals become even less bound (cf. the atomic case in Fig. 6) and their orbitals become more expanded, sampling better the potential field exerted by the ligands and acquiring, therefore, a larger (crystal-field) splitting between e^{CFR} and t_2^{CFR}. Because of their generic evolution from the impurity atomic d orbitals, perturbed by the crystal field, we refer to these levels as "crystal-field resonances" (CFR). We see that much like the situation in free ions (Fig. 6), the binding energies of these $3d$-related orbitals decrease as the atomic number decreases, reflecting primarily the weakening of the $-Z/r$ Coulomb attraction. However, whereas the slope of this decrease in free ions is large (1—3 eV per atomic number, cf. Fig. 6), the slope is considerably reduced for these species as impurities (e.g., ~ 0.5 eV for impurities past Ni). This is a clear manifestation of the formation of new chemical bonds between the impurity and the host atoms that stabilize the impurity binding energy relative to its free-ion form. Initially, for Ga $3d$, Zn $3d$, and Cu $3d$, these bonds are weak due to the sizable mismatch between these $3d$ —orbital energies and the (phosphorous-derived) valence-band energies. Hence, the e^{CFR} and t_2^{CFR} appear as narrow and deep resonances with little p-d hybridization and a steep decrease in their binding energies with atomic number. As we continue to go backward in the Periodic Table, the lighter impurities have smaller binding energies; the availability of host states of the same symmetries and compatible energies leads then to the formation of broad and heavily (p-d) hybridized resonances (i.e., TA $3d$—host $3p$ bonding combinations), with a slower rate of decrease in binding energy with Z (cf. Table IV). As we approach the low-Z limit of the series, we see that the energy of the t_2^{CFR} level becomes pinned inside the valence band (at about $E_v - 1$ eV), whereas the e^{CFR} level emerges into the band-gap region, first for GaP:Fe (the "e Threshold" in Fig. 9). It then gives rise to the acceptor states of GaP:Fe and GaP:Co. Hence, *the levels that constitute the deep acceptor states of these impurities are generically the same type of levels that give the XPS signal of pure GaP at $E_v - 18.5$ eV.* It is hoped indeed that the concentration of TA impurities in such semiconduc-

TABLE IV. Calculated energy levels (using transition-state acceptor occupation numbers) for the three main impurity-induced defect levels in GaP. Values given in eV relative to the valence-band maximum.

Impurity	t_2^{DBH}	e^{CFR}	t_2^{CFR}
Cr	2.02	0.6	-1.2
Mn	1.74	0.45	-1.1
Fe	1.2	0.13	-1.2
Co	0.66	-0.20	-1.65
Ni	0.26	-1.16	-2.6
Cu	0.10	-3.25	-4.15
Zn	0.02	-6.4	-6.4
Ga		-13.1	-13.1

tors could be eventually raised (e.g., by implantation) to the point where an XPS determination of the e^{CFR} and t_2^{CFR} levels for TA$\neq$Ga would become possible. [Note, however, that large relaxation effects, e.g., ~ 5 eV for GaP:Ga, are expected to lower the energies (Fig. 9). Furthermore, the attractive potential attendant upon formation of a hole in these states is predicted[59(d)] to form impurity-bound core excitons in the gap.[59(d)]]

The reason for the pinning of the t_2^{CFR} level inside the valence band has been discussed previously[59(c)] for Si:TA. The same mechanism, namely repulsion by conduction-band states of t_2 symmetry and attraction by the t_2 valence-band states having a peak in their (t_2-projected, substitutional) local density of states near $E_v - 1$ eV, is operative here. Inspection of their wave functions indeed suggests that, whereas at the high-Z limit the t_2^{CFR} states are highly localized pure $3d$ orbitals, at the low-Z limit they are dominated by these more extended, hostlike p orbitals. Since, however, there are fewer host states of substitutional e symmetry at this energy range, the nonbonding e^{CFR} level has a weaker interaction with the host states and, hence, can penetrate the band gap, but remains $3d$-like throughout the $3d$ series. Presumably it is pinned at higher energies (where a large density of host e states is available). This will occur for impurities lighter than Cr. This pinning mechanism is different[97(b)] from the vacancy-level pinning suggested by Hjalmarson et al.[97(a)]

Figure 10 depicts the radial components of the e^{CFR} wave function for a few impurities. The $l=2$ ("d-orbital") part [Fig. 10(a)] is dominant, exhibiting an atomiclike behavior in the central cell, with a rapid attenuation in amplitude as we move to lighter impurities. The next-higher, symmetry-allowed angular momentum component ($l=4$) is small in the central cell and delocalizes through the crystal [Fig. 10(b)]. Population analysis (defined in Ref. 58) shows that the localization of the e^{CFR} level within the nearest-neighbor sphere ranges from 99% for GaP:Zn to 75% for GaP:Cr. The t_2^{CFR} level shows a similar localization at the high-Z limit (97% for GaP:Zn), but a lower localization at the low-Z limit (45% for GaP:Cr), due to massive hybridization with the t_2-like host states.
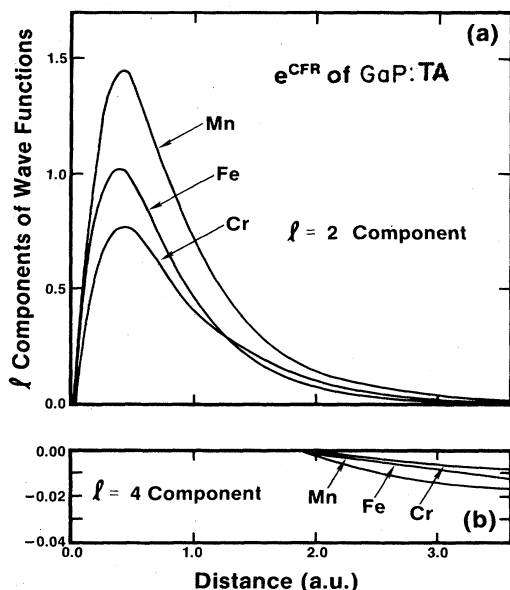
FIG. 10. Radial components of the e^{CFR} wave functions of Mn, Fe, and Cr impurities in GaP. (a) $l=2$ (d-orbital) components; (b) $l=4$ (g-orbital) components.

2. The t_2 dangling-bond hybrid

The bonding orbital t_2^{CFR} has an antibonding counterpart in the form of the t_2^{DBH} orbital. At the high-Z limit, where the atomic $3d$ orbitals are far deeper than the (anion-derived) host t_2 orbitals, there is little interaction between them; hence the p-like antibonding t_2^{DBH} orbital is just above the VBM. It is bound by a small central-cell potential (e.g., 0.02 eV in GaP:Zn) and by the effective-mass-like screened Coulomb tail [~ 0.05 eV (Ref. 8)], leading to a rather shallow single-acceptor level for GaP:Zn. As we move to lighter impurities, the orbitals of the impurity atom become closer to those of the host t_2 states, leading to a stronger repulsion and to the appearance of the t_2^{DBH} level in the center of the gap. At this range the t_2^{DBH} orbital contains larger proportions of d character. Because of the larger band gap of GaP compared with Si, the t_2^{DBH} state penetrates the conduction band in Si:Fe, Si:Mn, and Si:Cr, whereas these states are still in the gap of GaP. Since the t_2^{DBH} state evolves generically from the host dangling bonds around the impurity site, hybridized with the impurity d states, we refer to it as the "dangling-bond hybrid." The t_2^{DBH}-e^{CFR} splitting has been referred to, following Ludwig and Woodbury,[53(a)] as the "crystal-field splitting." Hence, this conventional Ludwig-Woodbury crystal-field splitting starts up for GaP:Ga at $E_{\text{VBM}}-E_d$, i.e., equals about 13 eV, and ends up being 1.42 eV for GaP:Cr (using acceptor-state occupation numbers). We note, however, that the true atomically derived levels split by the crystalline potential are, in fact, the e^{CFR}-t_2^{CFR} pair.

The lowest $d \rightarrow d^{*}$ excitation involves the e^{CFR}-t_2^{DBH} pair (Figs. 1—5). Our results for this separation (Table IV) hence predict an increase in the excitation energy in going from Fe to Mn and Cr, as well as an increase in go-

ing from Co to Ni. These trends match the experimental observations [Figs. 1(a)—5(a)].

Figure 11 depicts the radial components of the t_2^{DBH} wave functions for a few impurities. Its $l=2$ ("d-orbital") component [Fig. 11(a)] resembles atomic $3d$ orbitals; however, being antibonding, these wave functions show orthogonality nodes in the central cell [around $r \cong 2$ a.u. in Fig. 11(a)]. The d component is strong for GaP:Fe, and decays somewhat on both sides of Fe in the Periodic Table, as the level acquires more p character. The p-orbital components [Fig. 11(b)] have maxima that fall in the shaded area of Fig. 11(b) for most impurities. As can be seen from this figure, the p-orbital components are considerably more delocalized than the d-orbital components, peaking around the TA—P bond center. Population analysis[58] reveals strong (80%) p character at both the Zn and Cr ends of the series, and substantial (50%) d character at the center of the series (Fe). Notice, therefore, that for impurities with substantial $3d$ character in their t_2^{DBH} state we would predict the VBM$\rightarrow t_2^{\text{DBH}}$ transition (an allowed $p \rightarrow d$ excitation) to have substantially higher intensity than the $t_2^{\text{DBH}} \rightarrow$ CBM transition (a forbidden $d \rightarrow s$ excitation). This is the opposite of what has been proposed by Vogl[53(b)] from his tight-binding model.
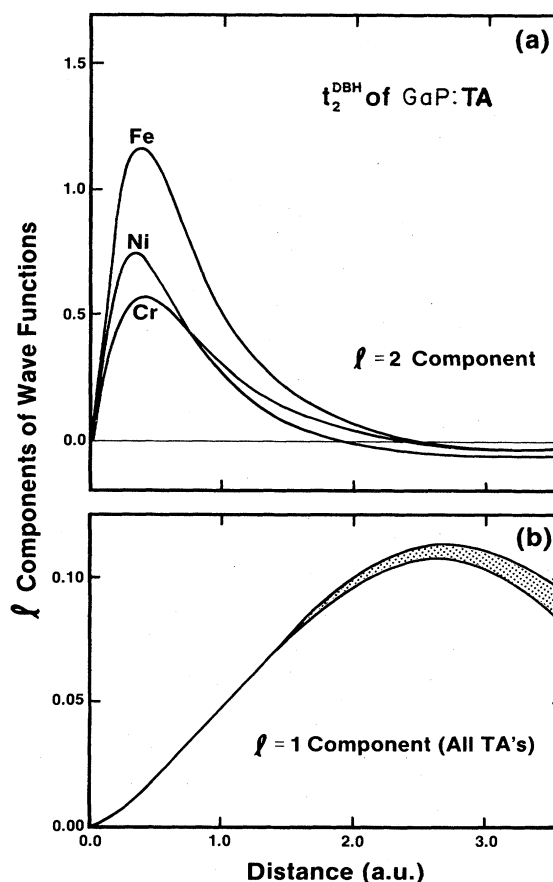

FIG. 11. Radial components of the t_2^{DBH} wave functions of Fe, Ni, and Cr impurities in GaP. (a) $l=2$ (d-orbital) components; (b) $l=1$ (p-orbital) components. The shading indicates the area where the $l=1$ component of all impurities falls.

The localization of the t_2^{DBH} in the nearest-neighbor sphere ranges from 2% for GaP:Zn to 50% in GaP:Fe. The remaining amplitude is delocalized through the crystal. The overall shapes of the e and t_2 impurity-induced orbitals (Figs. 10 and 11) hence suggest atomiclike $3d$ character at the *central cell*, but extended tails *throughout the crystal*. This dual behavior is central to the understanding of the apparent dichotomy between localized-like and extended-like impurity characteristics.[75] Being more expanded and hybridized than the e^{CFR} level, the $U^{(tt)}$ Coulomb repulsion energies are smaller than the $U^{(ee)}$ Coulomb repulsion energies (Table III). This is the reason why GaP:Cr can sustain the largest number of different charge states in the gap [A^+, A^0, A^-, and A^{2-}, cf. Fig. 1(a)] by altering the occupation numbers of its rather extended (singly occupied for A^0) t_2^{DBH} orbital. Since the optical $d \rightarrow d^*$ excitations involve electron transfer between t_2^{DBH} and e^{CFR} (Figs. 1–5), we see that such transitions are not really "intra-d" excitations, as they are often referred to,[7] but actually they redistribute charge between the impurity (e^{CFR}) and the ligands (t_2^{DBH}).

Other than the main, impurity-induced t_2^{CFR}, e^{CFR}, and t_2^{DBH} levels, Fig. 9 shows few other resonances. These include the t_2 resonance around the edge of the GaP heteropolar gap ($\sim E_v - 9.8$ eV) and two a_1 resonances, labeled in accordance with the analogous states observed in Si:TA [Refs. 59(a)–59(c)] as $a_1(1)$ and $a_1(3)$. The t_2 resonances are absent in the Si:TA system (having no heteropolar gap). All of these resonances have nearly hostlike orbitals and fade away as we proceed from Ni to the heavier impurities.

3. Comparison with other calculations

Recently, Gemma[98] used a cluster modification of the self-consistent numerical-basis-set, linear combination of atomic orbitals method[99] to study TA impurities of a 59-atom cluster of ZnO, ZnS, and GaP. He used a minimal (numerical) atomic basis set and sought a restricted type of self-consistency (charge and configuration self-consistency,[99] as opposed to unrestricted self-consistency[99]) by iterating over the Mulliken charges, within a model of superposition of spherical, atomiclike charge densities. For GaP:TA he finds an impurity-induced t_2 level above an e level, both residing in the fundamental band gap of GaP (3.05 eV, in his calculation). As in the present calculation, these levels arise up in energy in going from GaP:Ni to GaP:Cr. The Coulomb energies (calculated for GaP:Ni) are $U_{MF}^{(ee)} = 0.8$ eV and $U_{MF}^{(tt)} = 0.68$ eV, similar to those obtained here for GaP:TA (cf. Table III). Similarly, the t_2-e crystal-field splittings for the A^- center are comparable (0.7 eV for Co^{2+}, compared with our transition-state value of 0.86 eV, cf. Table IV). The significant differences, however, with the present calculation are as follows. (i) No valence-band resonances of the e^{CFR} or t_2^{CFR} type are reported by Gemma for any impurity (hence the band-gap levels found by Gemma are, most likely, related to these missing resonances). (ii) Gemma indicates that the t_2 gap levels do not have a dangling-bond character (i.e., t_2^{DBH}),

even for the heavier impurities, in contrast with the present work, as well as with other cluster calculations reported for similar systems[94,100] (e.g., GaAs:TA). (iii) Since no multiplet corrections are included, the comparison of his calculated results with experiment differs from ours (e.g., in the absence of multiplet stabilization, he concludes that the calculated t_2 level for Ni^{1+} is much too high relative to experiment).

No other calculations exist, to our knowledge, on GaP:TA. MS$X\alpha$ cluster calculations on GaAs:TA (Ref. 100) exhibit levels analogous to our t_2^{DBH}, e^{CFR}, and t_2^{CFR} and additional (unexplained) band-gap levels of a_1 symmetry. For the heavy impurities, substantially different results are obtained for the deep t_2^{CFR} and e^{CFR} levels, depending on the choice of cluster boundary conditions [$E_v - 18$ eV and $E_v - 5$ eV for GaAs:Cu in Refs. 100(a) and 100(b), respectively].

In Sec. VI A 2 we discussed Hemstreet's[94] cluster calculation of $3d$ impurities in InP and showed that the significant differences with our QBCF results on the same system are understandable in terms of the neglect[94] of both next-nearest-neighbor interactions (e.g., Fe-In, the only strong interaction that e orbitals experience) and the non-spherical potential terms. Recently,[100(c)] Hemstreet extended the same calculation to InP:Mn, InP:Co, and InP:Ni. He also finds, in addition to the strongly localized e^{CFR} level, a hostlike e level that occurs for InP:Co inside the gap. He uses this level to calculate the acceptor energy

$$[Co^{3+}, A^0, {}^5E, e^3t^3] \rightarrow [Co^{2+}, A^-, {}^4A_2, e^4t^3]$$

(cf. Fig. 4), and reports excellent agreement with experiment. We find (as well as others[53(b),19]) no impurity-induced hostlike e level at this energy range in any of our calculations (cf. Fig. 9).

This level can be traced to a hostlike e level that exists in Hemstreet's unperturbed cluster near the top of the valence band, similar to that observed in other cluster calculations.[100(a)] No such level exists in our substitutionally projected host density of states. We hence suspect that his impurity-induced e level is largely a consequence of the misrepresentation of the correct energy distribution of host states by his small-cluster model (TAP$_4$H$_{12}$). Indeed, by symmetry, e states in tetrahedral systems form bonds only with the next-nearest neighbors, which are represented in Hemstreet's calculation by hydrogen atoms.

In addition to the one-electron calculation, Hemstreet also reports the inclusion of multiplet corrections using the method of Fazzio, Caldas, and Zunger[52] (different from the pioneering method developed originally by Hemstreet and Dimmock,[94(b)] which was also reported[94(a)] to be the method used in the InP:Fe work[94(a)]. In this application he replaces our λ_e^2 and λ_t^2 by the fraction of d character enclosed in the impurity muffin-tin spheres in the e and t_2 gap orbitals, respectively. While the multiplet corrections found in this way improve the agreement with experiment, the magnitude of these corrections are about half of what we find, and lead incorrectly to a low-spin ground state[101] (i.e., instead of the observed high-spin ^5E state of Fe^{2+}).

4. Transition-metal phosphides
as a bulk analog to GaP:TA

It is interesting to note the similarity between the impurity-induced levels in GaP:TA and their "concentrated impurity limit," i.e., bulk transition-metal phosphides,[69] such as VP, CrP, and MnP. First, notice that all transition-metal phosphides attain a coordination number larger than 4 (akin to the unrelaxed GaP:TA impurity system) by adopting either the hexagonal ($B8_1$) NiAs structure (e.g., VP) or the orthorhombic ($B31$) MnP structure (all remaining phosphides). In this respect, the structure of GaP:TA would appear to be unstable with respect to increased metal concentration. Indeed, these systems show a limited solubility, until one approaches near to the 50%—50% stoichiometry that permits periodic arrangements with higher coordination. There is a striking analogy, however, between the qualitative features of the band structure of bulk phosphides and their dilute-impurity limit discussed here (Fig. 9). The band structure of transition-metal phosphides[102—104] shows, at low energies, a phosphorous $3s$ band (analogous to the lower valence band between $E_v - 9.8$ eV and $E_v - 12.4$ eV in Fig. 9), separated by a heteropolar gap from the upper valence band above it. The upper valence band consists first of the bonding combinations of P $3p$ and TA $3d$ orbitals (i.e., a t_2^{CFR}-like band) and the antibonding P $3p$—TA $3d$ bands (a t_2^{DBH}-like band). A narrow $M^{(3d)}$ $3d$—like nonbonding band (e^{CFR}-like) is also identified. The different properties of the TA phosphides are explained[69,102—104] in terms of the location of the Fermi energy E_F relative to these bands. For MnP, the Fermi energy E_F for the majority-spin states lie in the t_2^{DBH}-like antibonding band, whereas the E_F for the minority-spin states lies in the narrow nonbonding e^{CFR}-like band. The partial occupation of the localized e^{CFR}-like states gives rise to a substantial exchange splitting, sizable saturation moments [e.g., $1.29\mu_B$ in MnP (Ref. 105)], and a metallic behavior. In lighter-transition-metal phosphides, such as ScP,[103,104] the Fermi energy lies below the narrow nonbonding e^{CFR}-like band, but above the bonding band. Hence, despite notable structural differences, the electronic bands of TA phosphides resemble generically the impurity-induced states in GaP:TA.

C. Quasiparticle energy-level diagram

We have seen that the coupling of various one-electron configurations through the (anisotropic) interelectronic interactions invalidates the analogy between one-electron energy-level diagrams and the multiplet-dominated excitation and ionization energies. Nevertheless, such approximate diagrams[7,53(a),64] have been constructed in the past and have been extremely useful in summarizing a large amount of data. Having identified through our multiplet theory the predominant one-electron configuration for each multiplet in the various ionized and excited states, and having calculated the chemical trends in the electronic structure of these one-electron levels, we are in a position to construct a schematic quasiparticle diagram for

GaP:TA (Fig. 12). The quasiparticle energies correspond, in principle, to the sum of the bare orbital energies (cf. Fig. 9) and the spin and space correlation self-energies (whose differences are depicted in Fig. 7). All quasiparticle levels in Fig. 12 are occupied in increasing order of energy, with no unoccupied states below an occupied state (as opposed to the mean-field energy diagram in Fig. 9). Hence, excitations and ionizations are given as transitions from the highest occupied quasiparticle level to the lowest unoccupied quasiparticle level. Figure 12 summarizes a large number of results and observations on GaP:TA. It shows the predominant configuration for the A^0, A^-, and excited $(A^-)^*$ centers, their spin (S), and many-electron-term values. The optically and electrically active electrons are depicted as circles: open circles for A^0 centers, and circles enclosing a minus sign denoting the occupation of an A^- center. Straight arrows connecting quasiparticle energies and the VBM denote first-acceptor $H(-/0)$ transitions, and wavy lines denote the first intracenter $d \rightarrow d^*$ transitions. We next show how such a diagram can be used to interpret and systematize the observed transitions in terms of up-spin (t_+, e_+) and down-spin (t_-, e_-) quasiparticles states.

We start at the lower left-hand corner with GaP:Ga with its deep $t_\pm^{CFR}$ and $e_\pm^{CFR}$ levels, having, at this limit, a vanishingly small crystal-field splitting and no exchange-correlation (XC) splitting ($t_+^{CFR} = t_-^{CFR}$, $e_+^{CFR} = e_-^{CFR}$). The $t_\pm^{CFR}$ states remain fully occupied throughout the $3d$ series, and, hence, they are optically, electrically, and magnetically inactive. Since they represent bonding combinations, they contribute, however, to the chemical stability of the TA-host bond. Their electronic relaxation, attendant upon excitations and ionizations of the higher-energy levels, controls the magnitude of these transition energies. These levels were not recognized in the classic Ludwig-Woodbury model.[7,53(a)]

The $t_\pm^{DBH}$ states start at the GaP:Ga limit as fully occupied and unpolarized hostlike states near the VBM and acquire XC splitting as they are gradually depopulated, moving toward the GaP:V limit. The $t_\pm^{DBH}$ electrons are optically, electrically, and magnetically active. Since their Mott-Hubbard Coulomb energies are smaller than those of the more localized nonbonding $e_\pm^{CFR}$ states, spin-flip and electron-capture transitions require relatively little energy. This is a major contributing factor to the existence of numerous charge and excitation states involving these levels. For Zn, Cu, and Ni the first-acceptor transitions involve the upper (minority-spin), t_-^{DBH} states, whereas for Mn, and Cr, we predict the first-acceptor ionization to take place from the lower (majority-spin) states t_+^{DBH}. This is the reason why first-acceptor energies increase in the series Zn→Cu→Ni (0.07, 0.5, and 0.5—0.62 eV, respectively), and then, following a jump at Fe and Co, they increase again in the series Mn→Cr (0.4 and 1.12 eV, respectively). For the impurities between Ni and Cr, the $t_\pm^{DBH}$ states cannot be considered hostlike[53(b)] since they have a strong $3d$ component in the central cell.

The $e_\pm^{CFR}$ states start at GaP:Ga as fully occupied and unpolarized, highly localized levels near the $t_\pm^{CFR}$ pair. Being far more localized than the $t_\pm^{DBH}$ orbitals, they acquire larger XC splittings as they get progressively de-

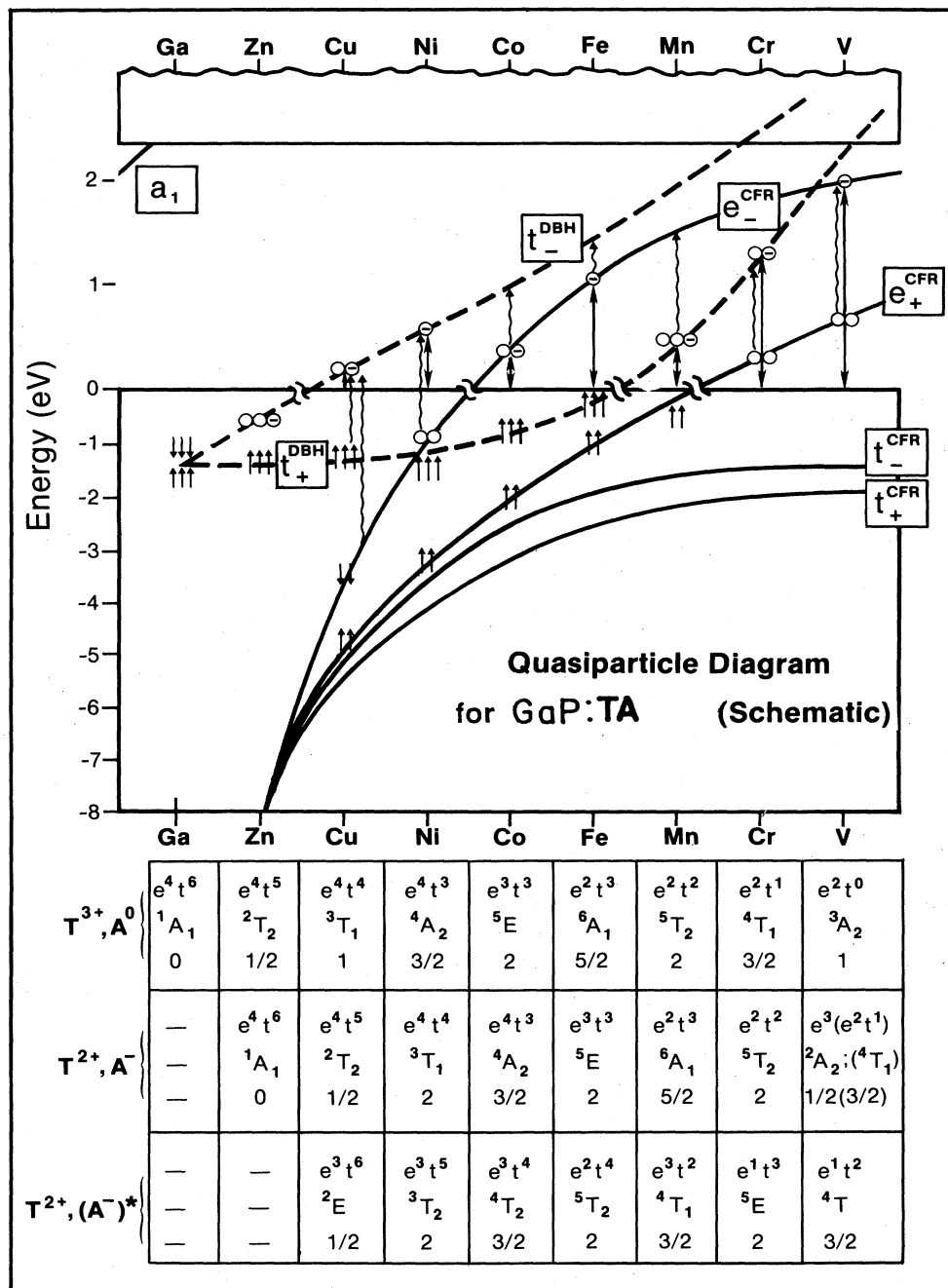| T^{3+},A^0	Ga	Zn	Cu	Ni	Co	Fe	Mn	Cr	V
	e^4t^6	e^4t^5	e^4t^4	e^4t^3	e^3t^3	e^2t^3	e^2t^2	e^2t^1	e^2t^0
	$^1A_1$	$^2T_2$	$^3T_1$	$^4A_2$	^5E	$^6A_1$	$^5T_2$	$^4T_1$	$^3A_2$
	0	1/2	1	3/2	2	5/2	2	3/2	1
T^{2+},A$^-$	—	e^4t^6	e^4t^5	e^4t^4	e^4t^3	e^3t^3	e^2t^3	e^2t^2	$e^3(e^2t^1)$
	—	$^1A_1$	$^2T_2$	$^3T_1$	$^4A_2$	^5E	$^6A_1$	$^5T_2$	$^2A_2;(^4T_1)$
	—	0	1/2	2	3/2	2	5/2	2	1/2(3/2)
T^{2+},(A$^-$)*	—	—	e^3t^6	e^3t^5	e^3t^4	e^2t^4	e^3t^2	e^1t^3	e^1t^2
	—	—	^2E	$^3T_2$	$^4T_2$	$^5T_2$	$^4T_1$	^5E	^4T
	—	—	1/2	2	3/2	2	3/2	2	3/2

FIG. 12. Schematic quasiparticle energy-level diagram, summarizing the excitation and ionization processes in GaP:TA. The electrically active electrons are denoted by circles, where open circles correspond to the occupation of the neutral A^0 centers and a circle enclosing a minus sign corresponds to the occupation of the A^- centers. Straight arrows connecting quasiparticle levels with the VBM denote first-acceptor transitions, and wavy lines connecting the t_2^{DBH} with the e^{CFR} states denote the first intracenter excitations. The t_+^{CFR} and t_-^{CFR} levels (separated by the shaded area) are each occupied by three electrons. Note change in scale above the VBM. At the bottom of the figure we give the predominant one-electron configurations, and the term values and the total spin, respectively, for A^0, A^-, and $(A^-)^*$, respectively.

populated in going to lighter impurities. The acceptor transitions in GaP:Co and GaP:Fe (and possibly GaP:V) involve ionizations of the higher (minority-spin) e_-^{CFR} state, but no ionizations occur from the lower (majority-spin) e_+^{CFR} levels, which are always full. The reason that

the Ni acceptor is higher in the band gap than the Co acceptor, although the free-ion ionization energies[57] show the reverse trend, is, hence, that the former acceptor involves the t_2^{DBH} orbital, whereas the latter acceptor involves the e^{CFR} orbital (lower by Δ_{eff}). The Co and Fe ac-

ceptors are hence expected to show substantially different capture cross sections than the other $3d$ acceptors which involve the ionization of the t_+^{DBH} states. As opposed to their electrical inactivity, the e_+^{CFR} states would dominate the magnetic activity. Having two parallel spins and being highly localized, they would lead to the formation of local magnetic moments for Co, Fe, Mn and Cr.

The crystal-field splitting between t_+^{DBH} and e_+^{CFR} reaches a minimum at the center of the $3d$ series, and increases rapidly toward the GaP:V end. This suggests that somewhere between V and $_{22}$Ti this splitting will be sufficiently large to favor a low-spin configuration (i.e., t_+^{DBH} above e_-^{CFR}), leading, perhaps, to e^3 with $S = \frac{1}{2}$ instead of $e^2 t^1$ with $S = \frac{3}{2}$ for V^{2+}. This consideration does not apply to V^{3+} (a d^2 ion), for which there is no distinction between low and high spin. Experimental examination of our prediction of a low-spin ground state for T_r^{1+} or even V^{2+} would be important in establishing if all $3d$ impurities are uniformly high spin (as suggested from the LW model) or not (as suggested).

The e_+^{CFR} states are the most difficult ones to calculate reliably using the standard local-density formalism:[55,66,75,95] their exchange splitting is likely to be severely underestimated when e^{CFR} is empty, unless the self-interaction correction[76] is applied. This is so since the local-density formalism emphasizes incorrectly the difference between up and down spin, instead of the difference between occupied and unoccupied spin states. We cannot determine reliably if the e_+^{CFR} level is above the t_-^{CFR} level for the heavy impurities Zn—Co.

The lowest-energy intracenter excitations of the A^- centers can be divided into three groups, according to the quasiparticle states involved in the excitation process: (i) GaP:Ni, GaP:Co, and GaP:Fe, which involves $e_-^{CFR} \rightarrow t_-^{DBH}$ transitions, in which the charge is displaced from the impurity site towards the ligands while conserving spin. (ii) GaP:Cr, which involves a similar transition, but with reversed spin, i.e., $e_+^{CFR} \rightarrow t_+^{DBH}$. (iii) GaP:Mn, which involves the spin-forbidden transition $t_+^{DBH} \rightarrow e_-^{CFR}$, in which charge is removed from the ligands and displaced toward the impurity site. A fourth class of (less likely) nondisplasive transitions (i.e., within the same representation) could occur for GaP:Cu ($t_+^{DBH} \rightarrow t_-^{DBH}$) and the low-spin form of GaP:V ($e_+^{CFR} \rightarrow e_-^{CFR}$), both involving a loss of two spins. Since these are strongly forbidden, the next transition (e.g., $e_+^{CFR} \rightarrow t_-^{DBH}$ in GaP:Cu) may be observed instead.

Finally, we compare our model of Fig. 12 with other models. In the Ludwig-Woodbury (LW) model[53(a)] (applied to III-V compounds by Kaufmann and Schneider[7]), the t_+^{CFR} states were omitted. Although Ludwig and Woodbury have not identified the dangling-bond nature of t_2^{DBH} and the localized-impurity-like nature of e^{CFR}, they have envisioned the existence of t_2 and e gap levels and have deduced spin configurations by assuming that the t_+^{DBH} level is always below the e^{CFR} level (high-spin, or weak-field, limit). This was also suggested to be the case of Vogl[53(b)] (his ordering of the t_2^{DBH} and e^{CFR} levels is identical to that of Ludwig and Woodbury). It is clear, however, from our foregoing discussion, that this condition cannot be satisfied at the GaP:Ga limit (where the

e_2^{CFR} level is at $E_v - 18.5$ eV and the t_2^{DBH} level is near the VBM). We suggest that it is also not satisfied for the elements bordering Ga, i.e., for Zn and Cu. We think that at the opposite, low-Z limit (e.g., V, $_{22}$Ti), this high-spin sit-
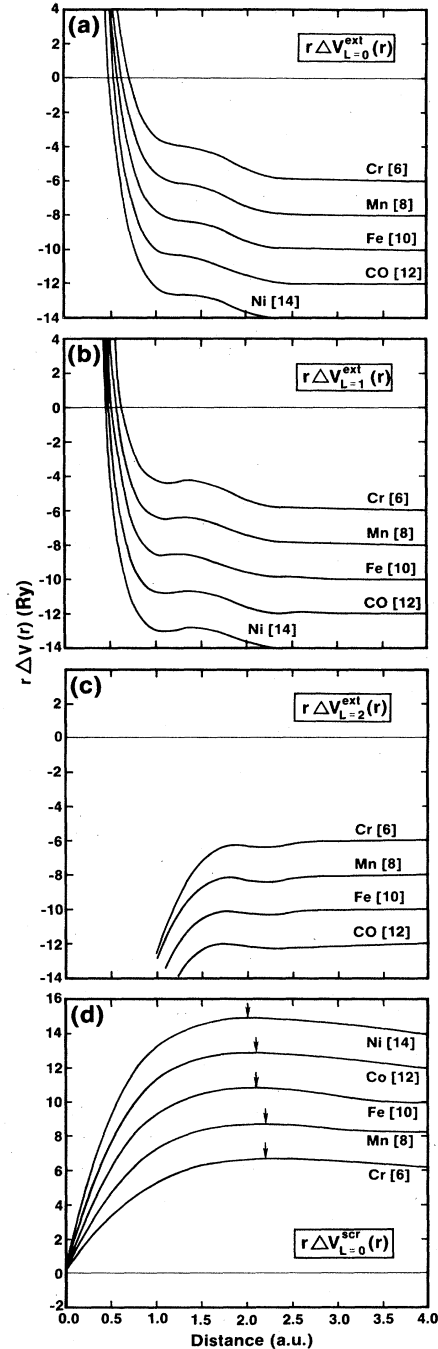

FIG. 13. r-multiplied pseudopotential perturbations for (a) $L=0$, (b) $L=1$, and (c) $L=2$ impurity pseudopotential components. The numbers in square brackets denote the asymptotic large-r limit that equals $-2\,\Delta Z = 2(Z_I - Z_{Ga})$. In (d) we show the r-multiplied spherical part of the host-crystal screening potentials. Arrows point to the positions of maximum in the screening function. Values in square brackets denote the large-r asymptotic limit $2\,\Delta Z$.

uation is also not likely to occur, as the large crystal-field splitting puts the t_+^{DBH} level above the e_-^{CFR} level. For the intermediate elements Ni, Co, Fe, Mn, and Cr, our model and that of Ludwig and Woodbury agree on the relative positions of the t_+^{DBH} and e_-^{CFR} levels.

D. Potentials and charge distribution

Having discussed the impurity-induced energy levels, we turn now to the discussion of the impurity-induced changes in the potentials and electron densities. Figure 13 depicts the pseudopotential perturbations $\Delta V^{\text{ext}}(r)$, i.e., the difference between the local Ga pseudopotential (with a valence charge $Z_{\text{Ga}} = 3$) and the nonlocal impurity pseudopotentials (with valence charges Z_I). When the difference is multiplied by r (Fig. 13), we find an effective (r-dependent) impurity ionic charge that approaches, at the large-r limit [shown in Figs. 13(a)–13(c)], the point-ion value of $-2\Delta Z = 2(Z_{\text{Ga}} - Z_I) = -6$, -8, -10, -12, and -14, for $I = \text{Cr}$, Mn, Fe, Co, and Ni, respectively. Inside the Wigner-Seitz sphere the impurity perturbation is different from its point-ion limit ($-2\Delta Z$). Whereas for $L = 0$ and 1 this central-cell correction is positive in a small region, inside the impurity core[83] it is attractive over most of the Wigner-Seitz cell. The attractiveness is lesser for the s and p waves than for the d wave, giving rise, therefore, primarily to strong d-type impurity-induced states. The crystal responds to this external perturbation $\Delta V^{\text{ext}}(r)$ by setting up a screening potential $\Delta V^{\text{scr}}(r)$ reflecting changes in the interelectronic Coulomb repulsions and exchange-correlation interactions [Fig. 13(b)]. At large r, the screening effective charge $r\,\Delta V^{\text{scr}}(r)$ reaches the value $2\Delta Z$ [indicated in Fig. 13(b) in square brackets], cancelling the external point charge $-2\Delta Z$. We see that the distance over which this cancellation takes place (screening length) is rather short (~ 4–5 a.u.), highlighting the nondielectric response of the system to localized perturbations. This can be better appreciated from the effective inverse dielectric function[59(a)] $\epsilon_{l,L}^{-1}(r)$ given by

$$\frac{\Delta V_L^{\text{ext}}(r)}{\epsilon_{l,L}(r)} \equiv \Delta V_L^{\text{ext}}(r) + \Delta V_l^{\text{scr}}(r) \qquad (20)$$

and depicted in Fig. 14. Clearly, the spherical ($l = 0$) response to the d-wave ($L = 2$) external perturbation

FIG. 15. Charge density along the $\langle 111 \rangle$ and $\langle \bar{1}\bar{1}\bar{1} \rangle$ crystal directions for various substitutional TA impurities in GaP.

occurs on an atomic length scale. This short-wavelength screening implies that the impurity-induced charge fluctuation $\Delta\rho(\mathbf{r})$ recovers after a rather short distance from the impurity site. The charge density $\rho_I(\mathbf{r})$ of the GaP:TA system (Fig. 15) shows a characteristic $3d$-like behavior along the $\langle 111 \rangle$ and $\langle \bar{1}\bar{1}\bar{1} \rangle$ crystal directions, with a rapid attenuation in amplitude as one moves to lighter impurities. The charge fluctuation $\Delta\rho(\mathbf{r})$ $= \rho_I(\mathbf{r}) - \rho_H(\mathbf{r})$, representing the difference between the impure (I) and host (H) systems (Fig. 16), has a dom-
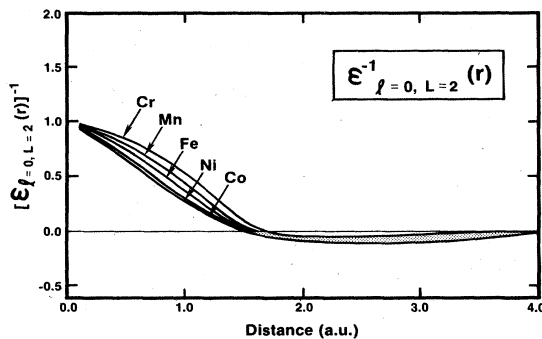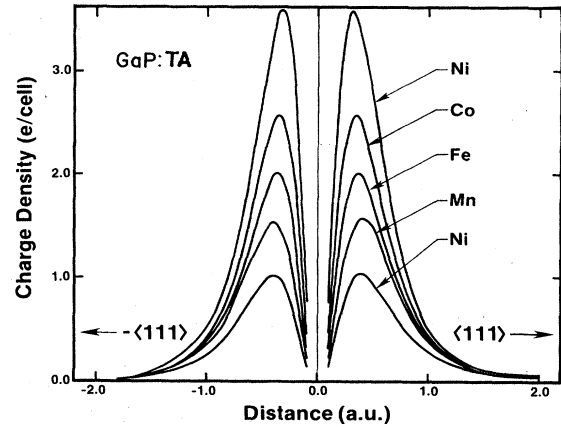

FIG. 14. Inverse of the effective spherical ($l = 0$) dielectric function for the $L = 2$ nonlocal pseudopotential perturbation [Eq. (20)]. The shading denotes the area common to all impurities.
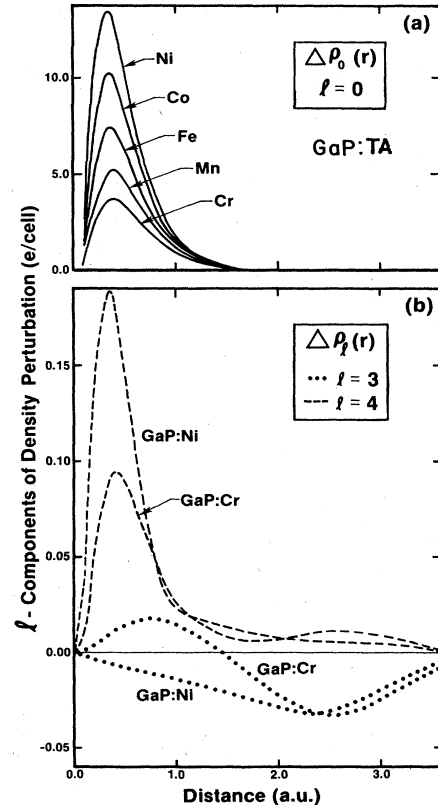

FIG. 16. (a) Spherical and (b) nonspherical components of the charge-density perturbation induced by different impurities in GaP.
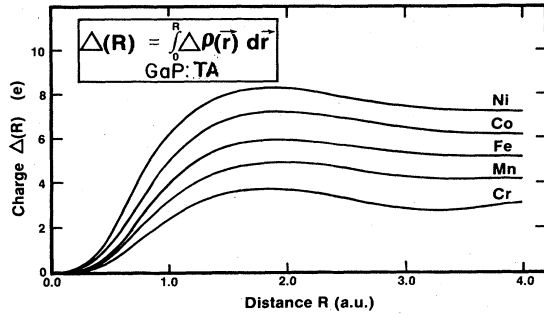
FIG. 17. Charge-accumulation functions, measuring the amount of charge density enclosed in a sphere of radius R around TA impurities in GaP. The large-r asymptotic limit is ΔZ.

inant spherical component $\Delta \rho_{l=0}(r)$ [Fig. 16(a)], as well as smaller, longer-range nonspherical components $\Delta \rho_{l=3}(r)$ and $\Delta \rho_{l=4}(r)$ [Fig. 16(b)], reflecting a change in the *anisotropy* of the bonding. When we integrate $\Delta \rho_{l=0}(r)$ up to a given distance R, we find the function

$$\Delta(R) = \int_0^R \Delta \rho_{l=0}(r) dr , \qquad (21)$$

which represents the rate at which charge is accumulated around the impurity. Clearly, for large R we expect to find $\lim_{R \to \infty} \Delta(R) = \Delta Z$, i.e., the total excess of impurity electrons over those of the Ga atom they replace. Figure 17 displays $\Delta(R)$ and shows that (i) the saturation limit is attained within a relatively short distance from the impurity site (~ 4–5 a.u.), consistent with the rapid screening evident from Figs. 13 and 14, and (ii) $\Delta(R)$ exceeds its asymptotic limit of ΔZ inside the central cell. This means that at short distances the impurity overscreens itself and compensates for this by having a negative charge fluctuation $\Delta \rho(r) < 0$ at a larger distance. This is the origin of the maxima in $r \Delta V^{\rm scr}(r)$ [where arrows are pointing in Fig. 13(d)]. We find that this "screening overshoot" is characteristic also of substitutional $3d$ impurities in silicon.[59(a)-59(c)] Notice that whereas the density fluctuation $\Delta \rho(r)$ recovers only after a relatively short distance from the center of the perturbation, the *individual* impurity-induced wave functions (e.g., the $t_2^{\rm DBH}$ and $e^{\rm CFR}$ orbitals of Figs. 11 and 10, respectively) can be rather extended. The reason for this is that whereas the antibonding gap-level orbitals are expanded, the bonding valence-band resonances become contracted so that the total fluctuation in density is short ranged. This interplay between the gap levels and the valence-band resonances can be better appreciated from Fig. 18. Here we have decomposed[59] the total impurity-induced charge $Q(R)$ into the contribution $\Delta Q_{\rm gap}(R)$ from the partially occupied gap-level orbitals and a contribution $\Delta Q_{\rm VB}(R)$ from the valence-band resonances. We display in Fig. 18 the R dependence of these contributions for GaP:Fe and InP:Fe, where we have normalized the limiting value $\lim_{R \to \infty} Q(R)$ to unity. We see that whereas the gap levels accumulate charge at a slow rate (i.e., the t_2 and e orbitals, contributing a charge $\Delta Q_{\rm gap}^{t_2}$ and $\Delta Q_{\rm gap}^{e}$, respectively, are not too localized), the valence-band resonances make up the difference by *decreasing* their contribution $\Delta Q_{\rm VB}(R)$ (past ~ 2 a.u.) at a faster rate. *The total charge*
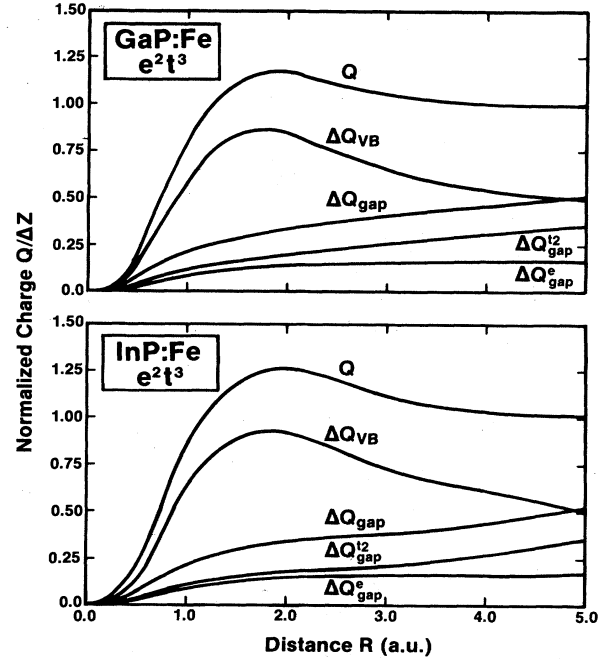

FIG. 18. Decomposition of the total impurity-induced charge $Q(R)$ into a contribution $\Delta Q_{\rm gap}(R) = \Delta Q_{\rm gap}^{t_2}(R) + \Delta Q_{\rm gap}^{e}(R)$ due to the gap levels, and a contribution $\Delta Q_{\rm VB}(R)$ due to the valence-band resonances, for GaP:Fe (upper) and InP:Fe (lower) systems.

$Q(R)$ hence attains its limiting value already inside the central cell. This self-regulating response of the valence-band resonances[59(c)] is the mechanism that reduces U, enabling different charge states to coexist in a relatively narrow energy range.

The opposing trends in the response of $\Delta Q_{\rm gap}$ and $\Delta Q_{\rm VB}$ to ionizations lead to a simple chemical picture. Whereas the neutral impurity A^0 has substantial charge on the ligands due to the partial delocalization of $t_2^{\rm DBH}$, when ionized to form A^+, charge flows (through orbital relaxation) from the ligands to the impurity, making up for much of the charge lost at the impurity site by its ionization. Hence, the *actual* charge on the impurity site will change by ionization to a lesser extent that what might be expected in ionic systems (e.g., FeF_2/F_eF_3). We hence predict Mössbauer isomer shifts for GaP:Fe to have an abnormally small change upon doping. This seems to explain the data of Seregin et al.[106]

It is interesting to compare the rates of charge accumulation for the same impurity in different host crystals. In Fig. 19 we provide such a comparison for a neutral Fe impurity in Si, GaP, and InP. We show the rate

$$Q_D(R) = \int_0^R \rho_I(r) dr$$

at which the defect (D) containing system accumulates charge, as well as the rate

$$Q_H(R) = \int_0^R \rho_H(r) dr$$

at which the pure host (H) crystal accumulates charge. Considering $Q_D(R)$, we may ask what is the radius R_S of a substitutional (S) impurity that encompasses its nomi-
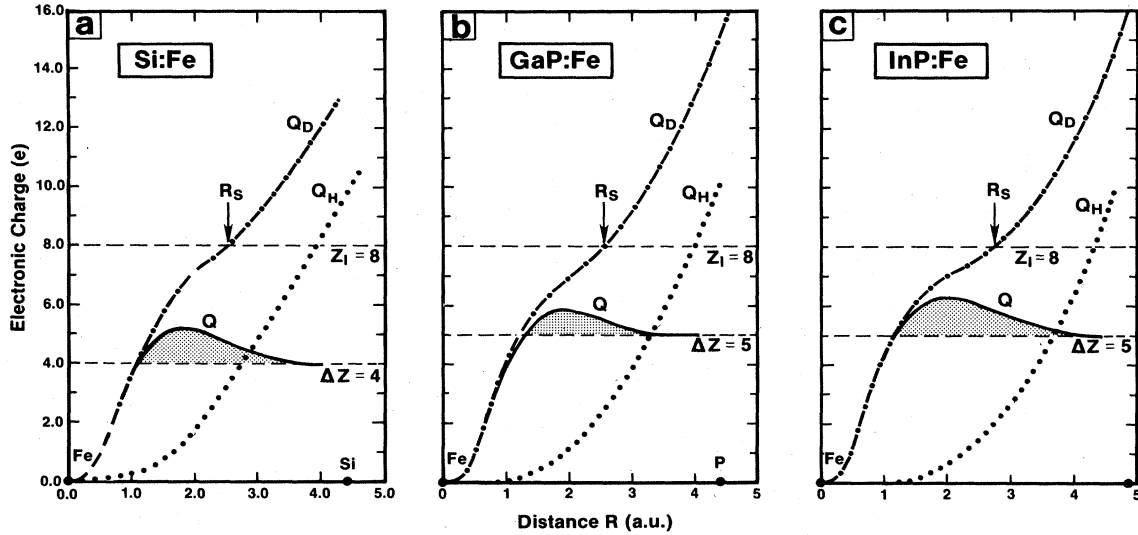
FIG. 19. We show for three impurity systems [(a) Si:Fe, (b) GaP:Fe, and (c) InP:Fe] the rate $Q_D(R)$ at which charge density is accumulated around the impurity site in the defect- (D) containing systems, the rate $Q_H(R)$ at which charge density is accumulated around a host-cation site in the pure-host (H) system, and the net impurity-induced charge $Q(R) = Q_D(R) - Q_H(R)$. The shaded areas denote regions where the impurity-induced charge exceeds its asymptotic limit ΔZ (screening overshoot). R_S denotes the effective impurity radius defined from $Q_D(R_S) \equiv Z_I$.

nal valence charge Z_I inside Q_D [i.e., define R_S from the condition $Q_D(R_S) \equiv Z_I$]? We find that this effective tetrahedral radius of bonded Fe is about the same in the three host crystals, ranging between 2.5 a.u. for GaP:Fe to 2.7 a.u. for InP:Fe. These values are close to the classical host-independent Slater-Bragg radius of tetrahedral ion (2.65 a.u., Ref. 107). We next show in Fig. 19 the impurity-induced charge-accumulation function $Q(R) = Q_D(R) - Q_H(R)$. As before, its asymptotic limit at larger r equals $-\Delta Z$, i.e., $8 - 4 = 4$ for Si:Fe and $8 - 3 = 5$ for GaP:Fe and InP:Fe. The shaded areas in Fig. 19 represent the regions of screening overshoot. We notice that in the more ionic system InP:Fe, where the screening is less effective, it takes a longer distance for $Q(R)$ to attain its "healed," asymptotic value. Further, in the highly covalent Si:TA system the screening overshoot is larger than in the heteropolar systems and occurs closer to the impurity center.

Finally, we have decomposed Q_D and Q_H at the nearest-neighbor radius $R = 4.4$ a.u. into their angular momentum (s,p,d) components, and inquire into the effective occupation numbers[59] q_s, q_p, and q_d of the TA impurity in GaP. In our previous study[59(a)−59(c)] of Si:TA, we found that q_d equals approximately the nominal valence Z_I, i.e., that both the atomic s and the d electrons become d-like in the impurity system. For GaP we find here that only $\frac{2}{3} - \frac{3}{4}$ of the s electrons are transferred into the d shell, and that the remaining charge resides in the impurity s and p orbitals. This is a manifestation of the higher Coulomb repulsion energies in GaP relative to Si, resisting a complete transfer of s electrons to the d shell. We further find that the impurity effective charge $Q(R)$ increases only by $(0.2 - 0.3)e$ as the formal charge state increases by unity (e.g., $A^0 \rightarrow A^-$). This is similar to the results obtained by us before[59(a)−59(c)] for Si:TA.

Three conclusions are evident. First, the actual impurity d-like charge q_d is considerably higher than that implied by the d symbolic crystal-field configuration $d^{p+q-3-k}$ (Table I), where k here is the charge state. For instance, whereas the symbolic crystal-field configuration for neutral (A^0) Cr^{3+} is d^3 and that for the negative center (A^-) Cr^{2+} is d^4, we find, for both configurations, $q_d = (5.3 \pm 0.3)e$. The reason for this is that in addition to the three $e^{CFR} + t_2^{DBH}$ gap electrons ("d^3") acknowledged by crystal-field theory, the impurity-induced valence-band resonances accomodate additional charge that resides on the impurity. Second, in contrast with the simple crystal-field picture, the impurity d charge does not increase by unity as its charge state increases by unity, precisely because the valence-band resonances reduce their amplitude in the impurity Wigner-Seitz cell to compensate for an increase in the occupation of the gap levels.[59] Finally, the net impurity ionic charge (the amount by which the positive core charge ΔZ exceeds the electronic charge inside the central cell) is of the order of $(0.1 - 0.2)e$ (the metal being positively charged), indicating rather small ionicity in these systems, in marked contradiction to the crystal-field picture (e.g., describing A^0 of Cr as a triply charged ion, Cr^{3+}).

VII. SUMMARY

Using the self-consistent quasiband crystal-field Green's-function approach[58] and the formulation of Fazzio, Caldas, and Zunger[52] for multiplet corrections, we have described the elements of the electronic structure of cation substitutional $3d$ impurities in GaP. Our main conclusions are the following:

(i) Despite substantial covalency, the impurity-induced states are rather localized inside the central cell, leading to

significant proportions of electron-electron multiplet corrections to the acceptor and donor ionization energies and to the Mott-Hubbard Coulomb repulsion energies. This is concluded from a systematic deconvolution of the observed transition energies into a mean-field one-electron piece and a multiplet correction piece. One-electron theory can, at best, reproduce the first component. Many-electron effects decay in their relative importance for heavier $3d$ elements (e.g., from Ni to Cu, being finally zero in Zn).

(ii) Cation substitutional transition-atom impurities in semiconductors have a universal energy-level scheme, showing a bonding, d-like t_2^{CFR} crystal-field resonance, an antibonding p-d—like t_2^{DBH} dangling-bond hybrid, and a nonbonding, d-like, e^{CFR} level between them. The impurity states that evolve from the atomic $3d$ orbitals are e^{CFR} and t_2^{CFR}, not e^{CFR} and t_2^{DBH}, as hypothesized by Ludwig and Woodbury. This pattern of energy levels is consistent with a simple three-level scheme, showing that the physically relevant (level-confining) gap is the tt^* gap (~ 3—4 eV), not the optical gap. Some acceptor transitions (e.g., in Zn, Cu, Ni, Mn, and Cr) evolve from the ionization of the t_2^{DBH} orbital, while others (Co and Fe) evolve from the ionization of the e^{CFR} orbital.

(iii) The nonmonotonic trend in the observed first-acceptor energies (e.g., minimum at GaP:Mn, local maximum at GaP:Fe) is largely a consequence of many-electron multiplet corrections (large and negative in GaP:Mn, smaller and positive in GaP:Fe). The one-electron e and t energy levels show a purely monotonic trend with Z.

(iv) Theory predicts the mean-field component of the first- and second-acceptor energies to within 0.2 eV from experiment for all impurities except Cr and Ni, for which a larger discrepancy (~ 0.5 eV) is evident. Since the predicted t_2^{DBH} energies for these two impurities (and to some extent also for GaP:Mn) are systematically higher than experiment, it appears that lattice relaxations (that have been observed to occur in these two systems) would lower the position of t_2^{DBH} by 0.2—0.5 eV. We predict a double acceptor for GaP:Co at $E_v + 2.4$ eV, i.e., just above the CBM.

(v) Mott-Hubbard Coulomb repulsion energies U in these systems are of the order of 1—1.6 eV (0.2—0.3 eV in Si:TA) and are significantly larger for e^{CFR} electrons than for t_2^{DBH} electrons. They are predicted by theory to within an accuracy of 0.2 eV, except for Cr, where they are calculated to be 0.5 eV too low. This suggests that the $A^-(T^{2+})$ state is stabilized by lattice relaxation more than the $A^{2-}(T^{1+})$ state is. If the discrepancy is entirely due to this effect, the net effect of the distortion is ~ 0.5 eV in GaP:Cr and ~ 0.2 eV in GaP:Ni. The large values of U invalidate the use of Koopmans theorem in these systems. Excitation energies between different $d \rightarrow d^*$ configurations are predicted to within ~ 0.3 eV, where theory overestimates systematically the interconfigurational crystal-field splittings for such transitions. The significant reduction in the Coulomb energies relative to their values in free ions (~ 20 eV) is a consequence of a charge self-regulating response, whereby valence-band resonances are reorganized spatially to accommodate popula-

tion changes in the gap levels. This self-regulating response explains the seemingly paradoxical dual nature of deep TA impurities in semiconductors: They are sufficiently localized to retain sufficiently large multiplet corrections, leading to high-spin ground states, yet they are sufficiently delocalized to accommodate numerous charge states within a narrow energy range.

(vi) Consistent with the self-regulating response and the smallness of U, we find very short (2—4 a.u.) screening lengths in the system, a fast recovery of the impurity-induced charge fluctuation, a partial $s \rightarrow d$ configuration crossover, and a screening overshoot. The net charge on most TA impurities in GaP is small [$(0.1-0.2)e$], indicating a rather minor role of ionicity. The self-regulating response further suggests that whereas the A^0 centers have significant charge on the ligands, upon ionization (forming A^+) charge flows from the ligands to the impurity. Hence, both A^0 and A^+ have comparable effective charges at the impurity core.

(vii) The impurity-induced levels in GaP:TA are generically relative to the (concentrated limit) band structure of Ta phosphides, much like the levels of Si:TA are related to the band structure of TA silicides.

(viii) The binding energies of the impurity-induced levels decrease when the impurity's atomic number decreases at a rate that is 5—10 times slower than that for free ions. This results from the formation of new transition-atom phosphide bonds.

APPENDIX A: OBSERVED TRANSITIONS IN GaP:TA

We review here the most reliably known ionization and excitation levels of $3d$ impurities in GaP used in this work.
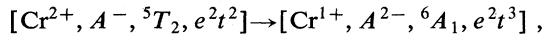
1. GaP:Cr

Figure 1(a) summarizes the best established electronic transitions in GaP:Cr. Chromium exists in this semiconductor in four charge states, A^+, A^0, A^-, and A^{2-}. The single-acceptor energy $(-/0) = E_v + 1.125$ eV was determined by Engeman and Hornung[9] using a two-step excitation of photoluminescence at 4.2 K. The excitation energy of the A^- impurity, $\Delta = 0.873$ eV, was determined by Abagyan et al.[10] Spectra were also given by Kaufmann et al.[11] and Kaufmann and Schneider[12] (see, however, White's contention[13]). The behavior of the zero-phonon line under stress suggests a tetragonal Jahn-Teller distortion. The double-acceptor energy $(-/2-)$ was determined to be at $E_v + 1.85$ eV by Clerjaud.[14] Brunwin et al.[15] found it at $E_v + 1.5$ eV, using photocapacitance

data, and Kaufmann and Koschel[11] suggested a minimum energy of $E_v + (1.15\pm0.07)$ eV from optically induced EPR. Recently, Kirilov et al.[16] contested this conclusion. We label, therefore, this transition in Fig. 1(a) as "tentative" (T). Chromium is the only $3d$ impurity in GaP that was found to have a donor $(0/+)$ transition. It occurs at $E_v + (0.5\pm0.1)$ eV, as suggested by Kaufmann and Schneider[17] using quenching data and EPR, and inferred by Gloriozova and Kolesnik[18] from their photocapacitance data. EPR data on GaP:Cr were given by Kaufmann and Schneider,[17] Kaufman and Koschel,[11] Kirillov et al.,[16] and Masterov et al.[19] The existence of a distortion in both A^0 and A^- (either Jahn-Teller, or due to aggregates) has been discussed on the basis of this data by Andrianov and Savel'ev.[20]

Using the $d \rightarrow d^*$ excitation data, we have fitted the spectra and found $\lambda_e = 0.856\pm0.08$, $\lambda_t = 0.787\pm0.08$, and $\Delta_{\mathrm{eff}} = 0.65\pm0.03$ eV. Using the parameters λ_e and λ_t we have calculated the multiplet spectra for each charge state. We give in Fig. 1(a) our assignment for these multiplet states, as well as the dominant one-electron configuration $e^m t^n$. We find that the single-acceptor transition $(-/0)$ corresponds to

$$[Cr^{3+}, A^0, {}^4T_1, e^2t^1] \rightarrow [Cr^{2+}, A^-, {}^5T_2, e^2t^2],$$
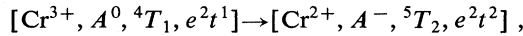
the double-acceptor transition $(-/2-)$ corresponds to

$$[Cr^{2+}, A^-, {}^5T_2, e^2t^2] \rightarrow [Cr^{1+}, A^{2-}, {}^6A_1, e^2t^3],$$

and the first-donor transition $(0/+)$ corresponds to

$$[Cr^{3+}, A^0, {}^4T_1, e^2t^1] \rightarrow [Cr^{4+}, A^+, {}^3A_2, e^2t^0].$$
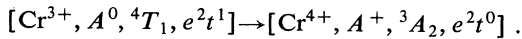
All three transitions are seen to involve a change in the occupation of the t orbitals. From the single-acceptor energy at $E_v + 1.12$ eV and the double-acceptor energy at $\approx E_v + 1.85$ eV, we find a Mott-Hubbard Coulomb repulsion energy of the t orbital in the A^- center to be $U^{(tt)}(A^-) \cong 1.85 - 1.12 = 0.73$ eV. From the single-acceptor energy at $E_v + 1.12$ eV and the single-donor energy at $E_v + (0.5\pm0.1)$ eV, we find a Mott-Hubbard Coulomb repulsion energy of the t orbital in the A^0 center to be $U^{(tt)}(A^0) = 1.12 - (0.5\pm0.1) = (0.62\pm0.1)$ eV. Our fit also predicts some yet unobserved spin-forbidden $d \rightarrow d^*$ transitions of the A^- center, e.g., the ${}^5T_2 \rightarrow {}^3T_1(t^2e^2)$ and ${}^3T_2(t^2e^2)$ transitions at 1.0 and 1.12 eV, respectively.

2. GaP:Mn

Figure 2(a) summarizes the data for GaP:Mn. Only two charged states (A^0 and A^-) were observed. Manganese has the lowest single-acceptor ionization energy of all $3d$ impurities in GaP. The energy of this $(-/0)$ transition at $E_v + 0.4$ eV was determined by the temperature dependence of the Hall coefficient by Abagyan et al.[21] and by Evwaraye and Woodbury.[22] The same value was obtained from infrared (ir) absorption associated with photoionizing A^0 into A^- and a hole.[21] The excitation energy of the A^- center was determined in luminescence by Vink et al.,[23] yielding a zero-phonon line at $\Delta = 1.53$ eV and a center at $\Delta = 1.34$ eV. ESR spectra of the A^- center were given by Title and Plaskett[24] and by Van

Engelen and Sie,[25] who have also observed by ENDOR the ^{55}Mn hyperfine splitting, the hyperfine interactions with the next-nearest Ga shell, and determined the cubic crystal-field parameters.

The fit to the optical excitation yields $\lambda_e = 0.86\pm0.08$, $\lambda_t = 0.858\pm0.08$, and $\Delta_{\mathrm{eff}} = (0.52\pm0.03)$ eV, and enables the assignment of the multiplets as given in Fig. 2(a). This fit also identifies some yet unobserved spin-forbidden $d \rightarrow d^*$ transitions of the A^- center, e.g., ${}^6A_1 \rightarrow {}^4E(t^3e^2)$, ${}^4A_1(t^3e^2)$, and ${}^4T_2(t^3e^2)$ at 1.78, 1.78, and 2.09 eV, respectively. The single-acceptor transition is assigned to

$$[Mn^{3+}, A^0, {}^5T_2, e^2t^2] \rightarrow [Mn^{2+}, A^-, {}^6A_1, e^2t^3],$$
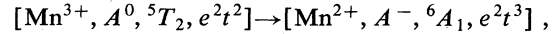
involving a change in the occupation of the t orbitals. The excitation of the A^- center is identified as the

$$[Mn^{2+}, A^-, {}^6A_1, e^2t^3] \rightarrow [Mn^{2+}, (A^-)^*, {}^4T_1, e^3t^2]$$
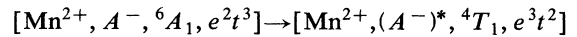
and is spin forbidden. It is found that both transitions are dominated by multiplet effects, where $\Delta E(0/-) = \Delta E_{\mathrm{MF}} + \Delta E_{\mathrm{MC}} = 1.59 + (-1.19)$ eV and $\Delta = \Delta_{\mathrm{MF}} + \Delta_{\mathrm{MC}} = 0.52 + 0.82$. Hence, the reason that Mn forms such a shallow acceptor in GaP with such a high $A^- \rightarrow (A^-)^*$ excitation energy is that the many-electron multiplet corrections lower the acceptor energy by 1.19 eV and raises its excitation energy by 0.82 eV.

3. GaP:Fe

Figure 3(a) summarizes the data for GaP:Fe. Iron has three charge states (A^0, A^-, and A^{2-}) in GaP. The single-acceptor energy $(-/0)$ has been determined to be $E_v + 0.86$ eV by Demberel et al.[26] by absorption of a p-i-n diode [supported also in Ref. 14(a)]. This value was higher than the older value of $E_v + (0.7\pm0.05)$ eV given by Andrianov et al.[27] from the temperature dependence of the Hall effect and the ir absorption at 300 K. Recently, Yang, Grimmeiss, and Samuelson[28] have observed the thermal emission rates, capture cross sections, and optical cross section, and have concluded that the enthalpy of transition is $E_v + 0.82$ eV, close to the value obtained by Demberel et al.[26] They estimated the optical threshold to be just below it, at $E_v + (0.78\pm0.05)$ eV.

The second acceptor $(-/2-)$ of GaP:Fe was determined by Suto and Nishizawa[29] to be at $\sim E_v + 2.25$ eV [supported by Ref. 14(a)] using Hall effect and EPR for identification. Using $(-/0)$ and $(-/2-)$ one finds a Mott-Hubbard Coulomb energy of $U(A^-) = 2.25 - 0.86 = 1.39$ eV. The excited state of the A^- center was observed by Andrianov et al.[27] at $\Delta = 0.413$ eV, as well as by Vasil'ev et al.[30] (stress splitting of zero-phonon lines) and by Clark and Dean.[31] More recently, West et al.[32] have measured the near-ir photoluminescence under unaxial stress, proving conclusively that the transition involves the crystal-field levels of the A^- center with minor Jahn-Teller energy shifts.
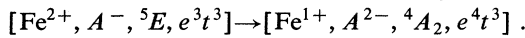
EPR data are available for the A^0 center (Ref. 33). ENDOR data have likewise been resolved by Teuerle and Hausmann,[34] who have suggested an interstitial site. EPR data for the A^{2-} center have been given by Kaufmann and Schneider.[35] The origin of this EPR was confirmed

by the ENDOR experiment of Kirillov and Teslenko.[33] Recently, Masterov et al.[36] have challenged the interpretation of Kaufmann and Schneider[37] that the A^{2-} center is a substitutional d^7 ion in the $^4A_2$ state. Instead, they suggested that the observed EPR might be due to a neutral A^0 central in the d^8 *interstitial* position in the $^3A_2$ state. In the absence of fine-structure experiments, it is not possible to distinguish between these $^4A_2$ and $^3A_2$ models from EPR. The A^- center has no EPR since it is a spin singlet.

Fitting the absorption spectra, we obtain $\lambda_e = 0.843 \pm 0.08$, $\lambda_t = 0.828 \pm 0.08$, and $\Delta_{\mathrm{eff}} = (0.45 \pm 0.03)$ eV. This fit predicts a number of yet unobserved $d \rightarrow d^*$ transitions of the A^- center, e.g., $^5E \rightarrow {}^3T_1(t^2e^4)$ to 0.75 eV, and a group of final states, ^3E, $^3T_1$, and $^3T_2$, all evolving from t^3e^3 and located at 1.22–1.28 eV. Calculation of the multiplet state for each of the three charged states yields the assignments given in Fig. 3(a). We identify the first-acceptor transition as

$$[\mathrm{Fe}^{3+}, A^0, {}^6A_1, e^2t^3] \rightarrow [\mathrm{Fe}^{2+}, A^-, {}^5E, e^3t^3]$$
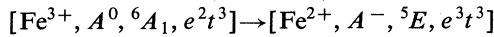
and the second-acceptor transition as

$$[\mathrm{Fe}^{2+}, A^-, {}^5E, e^3t^3] \rightarrow [\mathrm{Fe}^{1+}, A^{2-}, {}^4A_2, e^4t^3] \, .$$

Both transitions involve a change in the occupation of the e electrons. The value of the Mott-Hubbard Coulomb energy deduced above (1.39 eV), hence, corresponds to the e level of A^-. We note that the many-electron correction to the first-acceptor state is large $[\Delta E = \Delta E_{\mathrm{MF}} + \Delta E_{\mathrm{MC}} = (0.1 + 0.76)$ eV], whereas the many-electron correction for excitation is small $(\Delta E = \Delta E_{\mathrm{MF}} + \Delta E_{\mathrm{MC}} = [0.45 + (-0.037]$ eV).

4. GaP:Co

The experimental data for GaP:Co are summarized in Fig. 4(a). Cobalt has been observed in two charged states $(A^0$ and $A^-)$ in GaP. The single-acceptor $(-/0)$ energy was determined to be at $E_v + 0.41$ eV by Loescher et al.[37] using temperature dependence of the Hall effect. Using luminescence excitation, three excited states have been observed by Bishop et al.[38] and by Weber et al.[39] for the A^- state, at 0.559, 1.05, and 1.50 eV, similar to the results obtained earlier[40] by Baranowski et al. The EPR spectra of the A^- center have been observed by Weber et al.,[39] Kaufmann and Schneider,[41] and earlier by Suto and Nishizawa.[42]

The fit to the excitation spectra yields $\lambda_e = 0.831$, $\lambda_t = 0.759$, and $\Delta_{\mathrm{eff}} = 0.608$ eV. Using the λ_e and λ_t values, we calculated the multiplet states for A^0 and A^- given in Fig. 4(a). We identify the first-acceptor transition as

$$[\mathrm{Co}^{3+}, A^0, {}^5E, e^3t^3] \rightarrow [\mathrm{Co}^{2+}, A^-, {}^4A_2, e^4t^3] \, ,$$
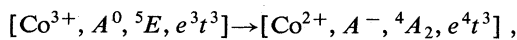
involving a change in the occupation of the e orbitals. We find a sizable many-electron correction to this acceptor state: $\Delta E = \Delta E_{\mathrm{MF}} + \Delta E_{\mathrm{MC}} = (-0.08 + 0.49)$ eV, whereas the many-electron correction for the first excited state is small: $\Delta E = \Delta E_{\mathrm{MF}} + \Delta E_{\mathrm{MC}} = [0.61 + (-0.05)]$ eV.

5. GaP:Ni

The experimental results for GaP:Ni are summarized in Fig. 5(a). Nickel appears in GaP in three charged states $(A^0, A^-, \text{and } A^{2-})$. The energy of the first acceptor $(-/0)$ was determined by Abagyan et al.[43] from the temperature dependence of the Hall effect to be at $E_v + 0.5$ eV, whereas Fung and Nicholas[44] have determined a somewhat questionable value of $E_v + 0.62$ eV, as they used the photoresponse of the photoconductivity [value supported by Ref. 14(a)]. The second acceptor $(-/2-)$ has been determined by Szaelska et al.[45] to be at $E_v + (1.55 \pm 0.1)$ eV using photocapacitance measurements. Abagyan et al.[43] give a similar value of $E_v + 1.5$ eV. Bishop et al.[38] found a value of $E_v + 1.77$ eV from luminescence excitation. Using the values of the single- and double-acceptor energies, a Mott-Hubbard Coulomb repulsion energy of $\sim(1.55 - 0.5) = 1.05$ eV can be deduced.

EPR data are available for the A^0 and the A^{2-} center. Data for the A^0 center are given by Kaufmann and Schneider,[41] whereas data for the A^{2-} center are given by Kaufmann et al.,[11] showing a moderate Jahn-Teller coupling. Recently, Ueda et al.[46] have described the ENDOR data for the A^0 center, where three shells of P sites and three shells of Ga sites could be resolved. The site symmetry was found to be substitutional tetrahedral. The two different charged states were recently reinvestigated by Ennen and Kaufmann[47] and by Ennen, Kaufmann, and Schneider.[48]

The absorption spectra of the A^- center were a subject of controversy. Baranowski et al.[49] observed three transitions at 0.705, 1.24, and 1.426 eV and assigned them to the excited states of the A^- center. Fitting these transitions, we obtain $\lambda_e = 0.748$, $\lambda_t = 0.714$, and $\Delta_{\mathrm{eff}} = 0.789$ eV. This fit identifies the three transitions as $^3T_1 \rightarrow {}^3T_2$, $^3T_1$, and $^3A_2$, respectively. Recently, however, Kaufmann et al.[11] and Ennen and Kaufmann[47] suggested that the lowest transition centered at 0.705 eV (zero-phonon line at 0.66 eV) does not represent an excited state of A^-, but rather that of A^{2-}, as is observed also by Noras and Allen.[50] They suggested that the correct lowest excitation of the A^- center is, in fact, at $\Delta = 0.58$ eV (zero-phonon line). This identification is supported by the luminescence-excitation spectra of Bishop et al.[38] (who, however, incorrectly claim that the excited states of A^- and A^{2-} overlap) and by the stress measurements of Hayes et al.[51] Using the three excitation energies 0.58, 1.24, and 1.426 eV, we have fitted the spectra, obtaining $\lambda_e = 0.817 \pm 0.004$, $\lambda_t = 0.800 \pm 0.003$, and $\Delta_{\mathrm{eff}} = (0.68 \pm 0.01)$ eV. The three transitions are assigned to $^3T_1 \rightarrow {}^3T_2$, $^3A_2$, and $^3T_1$, respectively, i.e., the order of the last two transitions is interchanged relative to the former fit based on older data.[49] We note that the latter fit is not perfect: the energy of the first-excited state [zero-phonon line (ZPL) observed at 0.58 eV] could not be lowered below 0.65 eV for any combination of the parameters (presumably, this can be due to the use of the ZPL rather than the absorption center for the fit). However, the experimentally deduced[11,47] value of 0.58 eV has been previously deduced from the higher levels and may well be

closer to our result of 0.65 eV. A mystery still remains as to why the excited state of A^- was not observed [it is observed in ZnS:Ni and ZnSe:Ni (Ref. 52)]. We display in Fig. 5(a) the experimental results as given by Kaufmann et al.,[11] together with the multiplet assignments obtained from our calculation. In square brackets we give the older and less tenable experimental results of Baranowski et al.[49] We have calculated the multiplet contribution to each excitation using both versions. Figure 5(b) gives the mean-field values calculated from Kaufmann's data, and

in square brackets we give the results of our calculation using, as input, the data of Baranowski et al. Clearly, the two sets of mean-field results differ substantially (e.g., the one-electron level for the single-acceptor transition is predicted to be 0.24 eV *below* the VBM using Kaufmann's data as input to the calculation, whereas if we use Baranowski's data, the predicted one-electron level is 0.14 eV *above* the VBM).

Further details about the fitting method we use are given in Ref. 52.

*Present address: Department of Physics, Indian Institute of Technology at Kanpur, Kanpur 208016, India.

[1]C. A. Liechti, Inst. Phys. Conf. Ser. 33A, 227 (1977).

[2]R. Zucca, B. M. Welch, P. M. Asbeck, R. C. Eden, and S. I. Long, in *Semi-Insulating III-V Materials,* edited by E. J. Rees (Shiva, London, 1980), p. 13.

[3]F. A. Bergh and P. J. Dean, *Light Emitting Diodes* (Oxford University Press, London, 1976).

[4]H. C. Casey and M. B. Panish, *Heterostructure Lasers* (Academic, New York, 1978).

[5]C. A. Liechti, IEEE Trans. Microwave Theory Techn. MTT-24, 279 (1976).

[6]H. J. Hovel, in *Semiconductors and Semimetals,* edited by R. K. Williamson and A. C. Beer (Academic, New York, 1975), Vol. 11.

[7]U. Kaufmann and J. Schneider, Adv. Electron. Electron Phys. 58, 81 (1983). See also, J. Schneider, in *Defects in Semiconductors II,* edited by S. Mahajan and J. W. Corbett (North-Holland, New York, 1983), 225.

[8]*Landolt-Börnstein Numerical Data and Functional Relationships in Science and Technology,* edited by O. Madelung, M. Schulz, and H. Weiss (Springer, Berlin, 1982), Vol. 17, p. 200.

[9]D. Engeman and Th. Hornung (unpublished work, quoted in Ref. 8, p. 200).

[10]S. A. Abagyan, G. A. Ivanov, Yu. N. Kuznetsov, Yu. A. Okunev, and Yu. E. Shanurin, Fiz. Tekh. Poluprovdn. 7, 1474 (1973) [Sov. Phys.—Semicond. 7, 989 (1974)].

[11]U. Kaufmann, W. H. Koschel, J. Schneider, and J. Weber, Phys. Rev. B 19, 3343 (1979).

[12]U. Kaufmann and J. Schneider, in *Festkörperprobleme (Advances in Modern Physics),* edited by J. Treuch (Pergamon/Vieweg, Braunschweig, 1980), Vol. 20, p. 87.

[13]A. M. White, Solid State Commun. 32, 205 (1979).

[14](a) Clerjaud (private communication); (b) also see B. Clerjaud, F. Gendron, and C. Porte, Appl. Phys. Lett. 38, 212 (1981); 38, 952(E) (1981).

[15]R. F. Brunwin, B. Hamilton, J. Hodgkinson, A. R. Peaker, and P. J. Dean, Solid State Electron. 24, 249 (1981).

[16]V. I. Kirillov, N. N. Pribylov, S. I. Rembeza, A. I. Spirin, and V. V. Teslenko, Fiz. Tekh. Poluprovdn. 17, 1149 (1983) [Sov. Phys.—Semicond. 17, 724 (1983)].

[17]U. Kaufmann and J. Schneider, Appl. Phys. Lett. 36, 747 (1980); Solid State Commun. 20, 143 (1976).

[18]R. I. Gloriozova and L. I. Kolesnik, Fiz. Tekh. Polyprovdn. 12, 117 (1978) [Sov. Phys.—Semicond. 12, 66 (1978)].

[19]V. F. Masterov, B. E. Samorukov, and V. K. Sobolevskii, Fiz. Tekh. Poluprovdn. 12, 2346 (1978) [Sov. Phys.—Semicond. 12, 1395 (1978)].

[20]D. G. Andrianov and A. S. Savel'ev, Fiz. Tekh. Poluprovdn.

14, 539 (1980) [Sov. Phys.—Semicond. 14, 317 (1980)].

[21]S. A. Abagyan, G. A. Ivanov, G. A. Koroleva, Yu. N. Kuznetsov, and Yu A. Okunev, Fiz. Tekh. Poluprovdn. 9, 369 (1975) [Sov. Phys.—Semicond. 9, 243 (1975)].

[22]A. O. Evwaraye and H. H. Woodbury, J. Appl. Phys. 47, 1595 (1976).

[23]A. T. Vink and G. G. P. Van Gorkon, J. Lumin. 5, 379 (1972).

[24]R. S. Title and T. S. Plaskett, Appl. Phys. Lett. 14, 76 (1969).

[25]P. Van Engelen and S. G. Sie, Solid State Commun. 30, 515 (1979).

[26]L. A. Demberel, A. S. Popov, and D. B. Kushev, Phys. Status Solidi A 52, 653 (1979).

[27]D. G. Andrianov, P. M. Grinstein, G. K. Ippolitova, E. M. Omel'yanovskü, N. J. Suchkova, and V. I. Fistul, Fiz. Tekh. Poluprovdn. 10, 1173 (1976) [Sov. Phys.—Semicond. 10, 696 (1976)].

[28]X. Z. Yang, H. G. Grimmeiss, and L. Samuelson, Solid State Commum. 48, 427 (1983).

[29]K. Suto and J. Nishizawa, J. Appl. Phys. 43, 2247 (1972).

[30]A. V. Vas'ilev, G. K. Ippolitova, E. M. Omel'yanovskü, and A. I. Ryskin, Fiz. Tekh. Poluprovdn. 10, 1201 (1970) [Sov. Phys.—Semicond. 10, 713 (1976)].

[31]M. G. Clark and P. J. Dean, Inst. Phys. Conf. Ser. 43, 291 (1979).

[32]C. L. West, W. Hayes, J. F. Ryan, and P. J. Dean, J. Phys. C 13, 5631 (1980).

[33]V. I. Kirilov and V. V. Tslenko, Fiz. Tverd. Tela (Leningrad) 21, 3209 (1979) [Sov. Phys.—Solid State 21, 1852 (1979)].

[34]W. Teuerle and A. Hausmann, Z. Phys. B 23, 11 (1976).

[35]U. Kaufmann and J. Schneider, Solid State Commun. 21, 1073 (1977).

[36]V. F. Masterov, S. I. Markov, L. P. Pasechnik, and V. K. Sobolevskii, Fiz. Tekh. Poluprovdn. 17, 1130 (1983) [Sov. Phys.—Semicond. 17, 711 (1983)].

[37]D. M. Loescher, J. W. Allen, and G. L. Pearson, J. Phys. Soc. Jpn. Suppl. 21, 239 (1966).

[38]S. G. Bishop, P. J. Dean, P. Porteous, and D. J. Robbins, J. Phys. C 13, 1331 (1980).

[39]J. Weber, H. Ennen, U. Kaufmann, and J. Schneider, Phys. Rev. B 21, 2394 (1980).

[40]J. M. Baranowski, J. W. Allen, and G. L. Pearson, Phys. Rev. 160, 627 (1967).

[41]U. Kaufmann and J. Schneider, Solid State Commun. 25, 1113 (1978).

[42]K. Suto and J. Nishizawa, J. Phys. Soc. Jpn. 27, 924 (1969).

[43]S. A. Abagyan, G. A. Ivanov, and G. A. Koroleva, Fiz. Tekh. Poluprovdn. 10, 1773 (1976) [Sov. Phys.—Semicond. 10, 1056 (1976)].

[44]S. Fung and R. J. Nicholas, J. Phys. C 15, 7355 (1982).

[45]H. R. Szaelska, J. M. Noras, and J. W. Allen, J. Phys. C 14, 4141 (1981).

[46]Y. Ueda, J. R. Niklas, J. M. Spaeth, U. Kaufmann, and J. Schneider, Solid State Commun. 46, 127 (1983).

[47]H. Ennen and U. Kaufmann, J. Appl. Phys. 51, 1615 (1980).

[48]H. Ennen, U. Kaufmann, and J. Schneider, Appl. Phys. Lett. 38, 356 (1981).

[49]J. M. Baranowski, J. W. Allen, and G. L. Pearson, Phys. Rev. 167, 758 (1968).

[50]J. M. Noras and J. W. Allen, J. Phys. C 12, L133 (1979).

[51]W. Hayes, J. F. Ryan, C. L. West, and P. J. Dean, J. Phys. C 12, L815 (1979).

[52]A. Fazzio, M. Caldas, and A. Zunger, Phys. Rev. B 29, 5999 (1984); 30, 3430 (1984).

[53](a) G. W. Ludwig and H. H. Woodbury, in Solid State Physics, edited by F. Seitz and D. Turnbull (Academic, New York, 1962), Vol. 13; P. Vogl, in Abstracts of the Fourth Lund International Conference on Deep Level Impurities in Semiconductors, Eger, Hungary (Hungarian Academy of Sciences, Budapest, 1983), p. 120.

[54]We use the local-spin-density formalism of W. Kohn and L. J. Sham [Phys. Rev. 140, A1133 (1965)] and the Perdew-Zunger form [J. P. Perdew and A. Zunger, Phys. Rev. B 23, 5048 (1981)] of the Ceperley-Alder [D. M. Ceperley and B. J. Alder, Phys. Rev. Lett. 45, 566 (1980)] correlation.

[55]B. H. Brandow, Adv. Phys. 26, 651 (1977).

[56]K. Wüthrich and R. G. Schulman, Physics Today 23, 43 (1970); A. Schejter, I. Aviriam, and T. Goldkorn, in Electron Transport and Oxygen Utilization, edited by Chien Ho (Elsevier, New York, 1982), p. 95.

[57]C. E. Moore, Natl. Bur. Stand. (U.S.) Ref. Data Ser. 34, (1970). The observed $T^{2+} \rightarrow T^{3+}$ ionization energies are 24.75, 28.14, 29.7, 30.95, 33.69, 30.65, 33.49, 36.16, 36.83, and 39.70 eV for Sc, Ti, V, Cr, Mn, Fe, Co, Ni, Cu, and Zn, respectively. The characteristic change in slope between $Mn(d^5 \rightarrow d^4)$ and $Fe(d^6 \rightarrow d^5)$ is seen to be 3.05 eV.

[58]U. Lindefelt and A. Zunger, Phys. Rev. B 26, 846 (1982).

[59](a) A. Zunger and U. Lindefelt, Phys. Rev. B 27, 1191 (1983); (b) Physica (Utrecht) 117B, 185 (1983); (c) A. Zunger and U. Lindefelt, Solid State Commun. 45, 343 (1983); (d) A. Zunger, Phys. Rev. Lett. 50, 1215 (1983); (e) A. Fazzio, M. Caldas, and A. Zunger (unpublished).

[60](a) J. Bernholc, N. O. Lipari, and S. T. Pantelides, Phys. Rev. B 21, 3545 (1980); (b) G. A. Baraff and M. Schlüter, ibid. 19, 4965 (1980).

[61]V. A. Singh, A. Zunger, and U. Lindefelt, Phys. Rev. B 27, 4909 (1983).

[62](a) A. Zunger and U. Lindefelt, Phys. Rev. B 26, 5989 (1982); (b) U. Lindefelt and A. Zunger, ibid. 30, 1102 (1984); (c) J. Phys. C 17, 6047 (1984).

[63]J. S. Griffith, The Theory of Transition Metal Ions in Crystals (Academic, New York, 1970). Also see C. J. Ballhausen, Introduction to Ligand Field Theory (McGraw-Hill, New York, 1962).

[64]S. Sugano, Y. Tanabe, and H. Kamimura, Multiplets of Transition-Metal Ions in Crystals (Academic, New York, 1970).

[65]M. Lannoo and J. Bourgoin, Point Defects in Semiconductors I (Springer, Berlin, 198), p. 131.

[66]A. Fazzio and A. Zunger, Solid State Commun. 52, 265 (1984).

[67]J. F. Mott, Metal Insulator Transitions (Taylor and Francis, London, 1974).

[68]G. W. Rubloff, Surf. Sci. 132, 268 (1983); O. Bisi and C. Calandra, J. Phys. C 14, 5479 (1981); P. S. Ho, G. W. Rubloff, and J. E. Lewis, V. L. Moruzzi, and A. R. Williams, Phys. Rev. B 22, 4784 (1980).

[69]B. F. Stein and R. H. Walmsley, Phys. Rev. 148, 993 (1966); K. Motizuki and K. Katoh, J. Phys. Soc. Jpn. 53, 735 (1984); R. Podloucky, J. Phys. F 14, L145 (1984).

[70]F. Herman and S. Skillman, Atomic Structure Calculations (Prentice-Hall, Englewood Cliffs, N.J., 1963).

[71]V. L. Moruzzi, J. F. Janak, and A. R. Williams, Calculated Electronic Properties of Metals (Pergamon, New York, 1978).

[72]J. W. Allen, in Semi-Insulating III-V Materials, edited by G. J. Rees (Shiva, London, 1980), p. 261.

[73]W. Kohn and J. R. Onffroy, Phys. Rev. B 8, 2485 (1973).

[74]H. L. Finston and A. C. Rychtman, A New View of Current Acid-Base Theories (Wiley, New York, 1982).

[75]H. Katayama-Yoshida and A. Zunger, Phys. Rev. Lett. 53, 1256 (1984).

[76]A. Zunger, J. P. Perdew, and G. L. Oliver, Solid State Commun. 34, 933 (1980); J. P. Perdew and A. Zunger, Phys. Rev. B 23, 5048 (1981).

[77]J. C. Slater, The Self-Consistent Field for Molecules and Solids (McGraw-Hill, New York, 1974), p. 51.

[78]W. Kohn and L. J. Sham, Phys. Rev. 140, A1133 (1965).

[79]P. Hohenberg and W. Kohn, Phys. Rev. 136, B864 (1964).

[80]We feel that this point was not appreciated by J. Jaros and P. J. Dean [Phys. Rev. B 28, 6104 (1983)] in their criticism of the work by T. N. Morgan on GaP:O [Phys. Rev. Lett. 49, 173 (1982)]. We suspect that many-electron contributions may be sizable for the GaP:O system, and that a treatment similar to the one carried here for GaP:TA may be necessary.

[81]U. Lindefelt and A. Zunger, Phys. Rev. B 24, 5913 (1981).

[82]V. A. Singh, A. Zunger, and U. Lindefelt, Phys. Rev. B 27, 1420 (1983).

[83]A. Zunger and M. L. Cohen, Phys. Rev. B 18, 5449 (1978); 20, 4082 (1979).

[84]J. R. Chelikowsky and M. L. Cohen, Phys. Rev. B 14, 556 (1976).

[85]C. Varea de Alvarez, J. P. Walter, M. L. Cohen, J. Stokes, and Y. R. Shen, Phys. Rev. B 6, 1412 (1971); D. E. Aspnes, C. G. Olson, and D. W. Lynch, ibid. 12, 2527 (1975).

[86]D. E. Eastman, W. D. Grobman, J. L. Freeouf, and M. Erbudak, Phys. Rev. B 9, 3473 (1979).

[87]L. Ley, R. A. Pollak, F. R. McFeely, S. P. Kowalczyk, and D. A. Shirley, Phys. Rev. B 9, 600 (1974).

[88]D. M. Wood and A. Zunger, Phys. Rev. B 31, 2570 (1985).

[89](a) G. P. Srivastava, J. L. Martins, and A. Zunger, Phys. Rev. B 31, 2561 (1985); (b) S. Froyen and M. L. Cohen, ibid. 28, 3258 (1984).

[90]H. G. Brühl and U. Pietsch, Phys. Status Solidi A 68, 689 (1981), and references therein.

[91]E. Fuess, Ann. Phys. (Leipzig) 80, 367 (1926).

[92](a) M. Scheffler (unpublished results); (b) typical breathing-mode relaxations for $3d$ impurities in semiconductors are calculated to be 4% or smaller, cf. Ref. 62(b).

[93]P. S. Bagus and U. Wahlgren, Mol. Phys. 33, 641 (1977).

[94](a) L. Hemstreet, Physica (Utrecht) 116B, 116 (1983), and private communication, for which are are grateful; (b) L. A. Hemstreet and J. O. Dimmock, Phys. Rev. B 20, 1527 (1979).

[95]A. Zunger, Phys. Rev. B 28, 3678 (1983).

[96]C. S. Wang and B. Klein, Phys. Rev. B 24, 3393 (1981).

[97](a) M. P. Hjalmarson, P. Vogl, D. J. Wolford, and J. D. Dow, Phys. Rev. Lett. 44, 810 (1980); (b) V. Singh, U. Lindefelt, and A. Zunger, Phys. Rev. B 25, 2781 (1982).

[98]N. Gemma, J. Phys. C 17, 2333 (1984).

[99]A. Zunger and A. J. Freeman, Phys. Rev. B **15**, 4716 (1977).

[100](a) A. Fazzio and J. R. Leite, Phys. Rev. B **21**, 4710 (1980); (b) L. A. Hemstreet, *ibid.* **22**, 4590 (1980); (c) L. Hemstreet, in *Proceedings of the Thirteenth International Conference on Defects in Semiconductors, Coronado, California, 1984,* edited by L. C. Kimmerling and J. M. Parsey (Metallurgical Society of AIME, Warrendale, Penn., 1985), p. 1043.

[101]A. Fazzio (private communication).

[102]A. Yanase and A. Hasegawa, J. Phys. C **13**, 1989 (1980).

[103]P. G. Perkins, A. K. Marawaha, and J. J. P. Stewart, Theor. Chim. Acta (Berlin) **59**, 555 (1981); **59**, 569 (1981).

[104]E. Wimmer, A. Neckel, and K. Schwarz, J. Phys. C **12**, 5441 (1979); **12**, 5453 (1979).

[105]A. Takase and T. Kasuya, J. Phys. Soc. Jpn. **47**, 491 (1979).

[106]P. P. Seregin, F. S. Nasredinov, and A. Sh. Bakktiyarov, Phys. Status Solidi B **91**, 35 (1979).

[107]J. C. Slater, *Symmetry and Energy Bands in Crystals* (Dover, New York, 1977), p. 55.